Energy Conversion and Management: X 23 (2024) 100629

Contents lists available at ScienceDirect

Energy Conversion and Management: X

journal homepage: www.sciencedirect.com/journal/energy-conversion-and-management-x

Metaheuristic Airflow control for vibration mitigation of a hybrid oscillating water Column-Floating offshore wind turbine system

Fares M'zoughi [a,*], Izaskun Garrido [a], Aitor J. Garrido [a], Manuel De La Sen [b]

[a] Automatic Control Group—ACG, Institute of Research and Development of Processes—IIDP, Department of Automatic Control and Systems Engineering, Faculty of Engineering of Bilbao, University of the Basque Country—UPV/EHU, Po Rafael Moreno no3, 48013 Bilbao, Spain
[b] Automatic Control Group—ACG, Institute of Research and Development of Processes—IIDP, Department of Electricity and Electronics, Faculty of Science and Technology, University of the Basque Country—UPV/EHU, Bo Sarriena s/n, 48080 Leioa, Spain

ARTICLE INFO

Keywords:
Airflow control
Floating offshore wind turbine
Adaptive neuro fuzzy inference system
Oscillating water column
Particle swarm optimization
Structural control

ABSTRACT

Unlike the fixed wind turbines, the structure of Floating Offshore Wind Turbines (FOWT) have the added motions of six degrees of freedom induced by the wind, wave and tidal loads. These motions lead to vibration and the degradation of the structure. This paper presents a novel approach to model and stabilize the FOWT by employing the Oscillating Water Columns (OWC) as active structural control system. The innovative concept involves designing a new floating barge-type platform with integrated OWCs on opposite sides of the platform to mitigate undesired oscillations of the system. These OWCs counteract the bending forces caused by wind on the tower and waves on the barge platform. To synchronize the opposing forces with the system's tilting, a proposed Particle Swarm Optimization with Decreasing Inertia-based Adaptive Neuro-Fuzzy Inference System (PSODI-ANFIS) airflow control strategy is employed. Through manipulation of the barge platform's pitch angle, the PSODI-ANFIS airflow control system adjusts the valves on either side, opening one and closing the other accordingly. Simulation results, compared with the standard FOWT as well as the Fuzzy-based airflow control system, demonstrate the effectiveness of the PSODI-ANFIS airflow control. It is shown to be superior in reducing platform pitching and the fore-aft translation of the top tower.

1. Introduction

Some immediate challenges posed by the global energy crisis have alleviated, however the energy markets, geopolitical landscape, and the world economy remain in a state of uncertainty, with the persistent risk of further disruptions. Although fossil fuel prices have receded from their 2022 peaks, market conditions are marked by tension and volatility. Ongoing conflicts in Ukraine, extending beyond the third year since Russia's invasion, are compounded by the looming threat of prolonged strife in the Middle East. The macroeconomic environment, which is now characterized by persistent inflation, high borrowing prices, and high debt levels, has a significant impact on the energy market. The energy markets are faced with difficulties as a result of these economic factors, which affect supply and demand dynamics. Sustaining inflationary pressures has the potential to raise production costs in the energy sector, impacting every aspect from distribution to extraction. Increased borrowing prices increase the cost of funding energy projects, which may discourage investment in renewable energy and new infrastructure. Furthermore, high debt levels might limit business investment and consumer spending, which lowers the energy demand overall. Therefore, the energy industry has to carefully manage these macroeconomic issues, adjusting strategies to reduce risks and take advantage of new possibilities in an uncertain economic landscape.

The creation and implementation of FOWT systems represents a revolutionary advancement in the field of renewable energy technology. FOWTs are made to float above the ocean's surface, in contrast to conventional fixed-bottom offshore wind turbines. This allows for the harvesting of wind energy in deeper seas where permanent structures are impractical. This invention has greatly increased the number of possible locations for wind energy generation by revealing enormous stretches of unexplored offshore wind resources. With the ability to be moored to the seabed, FOWTs' sophisticated floating platforms enable flexible installation in a range of marine situations. This flexibility helps with deployment in deep offshore areas by addressing logistical and technological issues. The capacity to grow and scale up turbine installations are two factors that lead to better energy absorption and efficiency. The development of FOWT systems underscores a commitment to

* Corresponding author.
E-mail address: fares.mzoughi@ehu.eus (F. M'zoughi).

https://doi.org/10.1016/j.ecmx.2024.100629
Received 2 February 2024; Received in revised form 8 May 2024; Accepted 18 May 2024
Available online 31 May 2024

Nomenclature

Abbreviations

ANFIS	Adaptive Neuro-Fuzzy Inference System
ANN	Artificial Neural Network
BP	Back-Propagation
DoF	Degrees of Freedom
EM	Error Mean
ESD	Error Standard Deviation
FCM	Fuzzy c-means
FFNN	Feed Forward Neural Network
FIS	Fuzzy Inference System
FOWT	Floating Offshore Wind Turbine
GP	Grid Partitioning
LCoE	Levelized Cost of Energy
LMA	Levenberg-Marquardt Algorithm
LSE	Least Square Estimation
MF	Membership Functions
MLP	Multi-Layer Perceptron
MSE	Mean Square Error
MSE	Mean Squared Error
OLE	Object Linking and Embedding
OpEx	Operational Expenditure
OWC	Oscillating Water Column
PSO	Particle Swarm Optimization
PSODI	PSO with Decreeing Inertia
PTO	Power Take- Off
RMSE	Root Mean Square Error
TMD	Tuned Mass Damper
WEC	Wave Energy Converter
WT	Wind Turbine

Symbols

d_p	Platform hydrodynamic damping
d_t	Tower damping
k_p	Platform stiffness
k_t	Tower stiffness
m_p	Platform mass
m_t	Tower mass
θ_p	Platform pitch angle
θ_t	Tower pitch angle
w_c	Chamber's inner width
l_c	Chamber's inner length
h_c	Chamber's inner height
S	Chamber's inner water free surface
H_t	Tower height
ρ_c	Water density
ρ_a	Atmospheric density
p_a	Atmospheric pressure
Φ	Dimensionless flow coefficient
r	Turbine mean radius
n	Blade number
b	Blade span
l	Blade chord length
a	Cross-sectional area
T	Total kinetic energy
V	Total potential energy
L	Lagrange operator
q_i	Generalized non-potential forces
I	Inertia moment
R	Distance from MC to tower base
M_{wind}	Bending torques induced by wind loads
M_{wave}	Bending torques induced by wave loads
f_{owc1}	Forces generated by OWC
V_{wind}	Wind speed
Z	Wave elevation
V_0	Chamber's undisturbed air volume
V_{OWC}	Instantaneous air volume
ω	Rotational speed
v_x	Axial speed
Q	Volume flow rate

diversifying the renewable energy portfolio and marks a crucial step toward achieving sustainable, carbon–neutral energy generation on a global scale.

The development and deployment of FOWT systems have brought attention to several issues, particularly concerning structural behavior influenced by wind-induced loads on the tower and wave-induced loads on the platform. These loads escalate stress, the risk of failures, potential damages, and maintenance expenses, thereby diminishing efficiency and overall lifespan. Various concepts have been introduced to alleviate these loads, categorized into two approaches. The first approach involves utilizing rotor thrust as a restoring torque to reduce FOWT pitching. This can be achieved by adjusting the pitch angle of the blades. J. Jonkman et *al.* conducted extensive investigations, developed the FAST tool, and created a baseline collective-pitch angle control for blade pitch in three main types of FOWTs, employing FOWT, employing a gain-scheduled PI control [1,2]. M.A. Lackner et *al.* [3] controlled the pitch of the blades by changing the rated rotor speed, inducing the generation of additional restoring torque. A. Staino et *al.* [4] employed a twofold control, merging passive pitch control and active tendons in the blade's structure to mitigate the aerodynamic loads. More recently, J. Yang et *al.* suggested a novel concept in [5], combining the advantages of a spar-type platform and a semi-submersible platform. The second technique for alleviating loads involves passive or or active structural controls. M.A. Lackner et *al.* [3] created FAST-SC, which incorporates structural control in FOWTs via the use of passive Tuned Mass Damper (TMD) mounted inside the nacelle. This introduces 2 Degrees of Freedom (DoF) of the TMD to the kinetic formulas. M.A. Lackner et *al.* in [6] optimized the TMD for a barge-type FOWT with the use of FAST-SC. N. Luo et *al.* treated in [7] the FOWT as a lump-like mass and utilized a Tuned Liquid Column Damper to decrease surge displacements. Y. Hu et *al.* [8] implemented active structural control with the use of a stroke-limited Hybrid Mass Damper with a linear-quadratic regulator.

Novel strategies for reducing wave loads on offshore wind farm platforms sometimes entail combining different energy converter technologies, such as tidal and wave technology. These other approaches take advantage of the dynamic forces found in oceanic settings to improve platform stability and also extract more renewable energy. To harness the energy found in ocean waves and tidal currents, offshore wind turbine platforms can strategically integrate Wave Energy Converters (WECs) with tidal turbines. Through the utilization of various renewable resources and energy mix diversification, offshore wind energy generation might potentially benefit from enhanced resilience and efficiency through the implementation of these integrated systems. Furthermore, combining wind turbines with wave and tidal converters can maximize the utilization of maritime resources and aid in the development of more sustainable and robust offshore energy infrastructure. Moreover, this approach allows companies to optimize the utilization of costly platforms by extracting energy from multiple sources simultaneously, leading to enhanced efficiency and cost reduction. Among the various combinations, wave and wind hybrid platforms stand out as the best esteemed and appropriate for deep offshore waters [9–12]. The incorporation of WECs with FOWT has been proposed and

has demonstrated promising outcomes. J.M. Kluger et *al.* [13] investigated the use of a WEC array with a spar-based FOWT known as OC3-Hywind. Z. Ma et *al.* explored the impact of typhoons on the aerodynamic performance of OC3-Hywind in [14]. A. Slocum et *al.* [15] examined the effects of employing outer and inner heaving WECs within the same floating system. M. Kamarlouei et *al.* [16] found that implementing a wave energy converter array could reduce oscillations in the system's heave and pitch modes. In a recent study, M.J. Khatibani et *al.* delved into the dynamics and energy extraction of a suggested novel hybrid mono-pile Wind Turbine (WT) in conjunction with two pitching wave energy converters [17]. However, it's worth noting that the methods presented have not yet incorporated OWCs in FOWTs using barge platforms.

WECs may play a crucial role in the stabilization of FOWTs by optimizing the design, the energy extraction and predicting wave conditions. Through optimization, WECs can efficiently harness wave energy, providing supplementary power to FOWTs while enhancing their stability. By strategically deploying WECs around FOWTs, the combined system can effectively mitigate the impacts of waves, reducing platform motions and enhancing overall structural integrity. In [18] N.M. Tom et *al.* studied a combined Oscillating Surge Wave Energy Converter (OSWEC) with control surfaces. The control surfaces allow for a variable device geometry that enables the hydrodynamic properties to be optimized. The design was shown to be effective at tuning the hydrodynamic characteristics to match the resonant frequency of the device to the dominant wave excitation frequency thus allowing for optimum power extraction in low-to-moderate sea states. Q. Li et *al.* analyzed the influence of various design parameters such as flap dimensions, submerged depth, incident wave direction, and water depth on the performance of the Self-Floating Oscillating Surge Wave Energy Converter (SF-OSWEC) in [19]. In [20] E. Amini et *al.* used metaheuristic optimization methods to investigate the effects of geometric factors on the performance of an OSWEC by optimizing the design parameters of the flap of the converter, in addition to the effects of hydrodynamic parameters. M. Neshat et *al.* proposed in [21] the enhancement of the performance of hybrid wave-wind energy systems consisting of a braceless semisubmersible platform and three torus-shaped WECs attached to the platform's side columns through a fast and adaptive chaotic multi-objective swarm optimization method.

This study proposes integrating OWCs with a FOWT to harness both wave and wind power, with a focus on stabilizing the floating platform of a 5 MW FOWT through the incorporation of OWCs [22–25]. The studied floating system involves the NREL 5 MW WT mounted on a barge platform. The objective is to introduce OWCs to the designated barge to mitigate undesired vibration of the system [24]. Stabilization is achieved through the control of air valves for each OWC, employing an airflow control method [26–28]. This approach enables the regulation of airflow and pressure within the capture chambers.

Since ocean waves are larger than nearshore waves, it is possible to assume that waves are large enough to consider the oscillating water free-surface inside the OWC chambers as one rigid body heaving inside the column along the vertical axis. Hence, it is possible to assume that the internal free surface inside the OWC's chamber behaves like a piston and the pressure is uniform according to the following assumptions:

- The ocean waves are large enough to make the water free-surface inside the chambers oscillate as the same body (piston).
- The water free-surface inside the chamber only oscillates along the chamber's vertical axis.
- The water free-surface is a rigid piston with a thickness that may be non-zero but the sum of the mass and added mass of the rigid piston is practically independent of its thickness.

The assumption is that the internal free surface inside the OWC's chamber behaves like a piston and the pressure is uniform.

The current paper proposes and implements a PSODI-ANFIS for airflow control, effectively managing the opening and closing of the integrated OWCs' air valves collectively. PSODI is used to enhance the obtained ANFIS model from the Fuzzy c-means (FCM) clustering. It has been considered because it is computationally efficient due to its simple structure and fewer parameters compared to other optimization algorithms, easy to implement and requires minimal parameter tuning, versatile and can be applied to various optimization problems, and is robust to noisy environments and can handle non-linear, non-convex, and discontinuous objective functions. The performance of the proposed PSODI-ANFIS airflow control strategy is assessed by comparing it with a Fuzzy-based airflow control in [23] and the standard barge FOWT.

The remaining sections of this paper are organized to Section 2, which provides detailed equations for the hybrid OWC and FOWT mathematical model. Section 3, which introduces the PSODI-ANFIS for airflow control. This strategy is developed to adjust the airflows and pressures inside the air chamber of the OWCs, contributing to the stabilization of the overall system. Section 4, which presents a comparative study of the structural behavior of the FOWT among three scenarios: the standard barge FOWT, the OWC-FOWT with a fuzzy control, and the OWC-FOWT with the PSODI-ANFIS control. And Section 5, which concludes the paper with some summarizing interpretations.

2. Novel hybrid wind-wave FOWT concept

This research study focuses on the stabilization of the FOWT depicted in Fig. 1. The study specifically examines the NREL 5-MW baseline WT mounted on an ITI Energy barge. The chosen platform is a square structure that has been commonly explored for load analysis and conceptual verification of floating WTs.

The studied WT is of the upwind type, featuring three blades and employing variable speed control as well as pitch control. The blades drive the generator situated inside the nacelle at the summit of the tower, positioned at an elevation of 90 m. The WT is affixed atop a squared ballasted barge base, anchored with catenary mooring lines to minimize drifting and enhance platform stability. Comprehensive parameters of the 5 MW wind turbine and the ITI Energy barge may be encountered in [1], with the most pertinent characteristics summarized in Table 1.

Despite the substantial surge displacement observed in barge platforms, research indicates that the pitch inclination of the barge platform has the most significant impact on bending of the tower [29]. Consequently, the pitching mode has been activated, while the surge motion has been disabled. This approach has demonstrated sufficient efficiency in controlling structural vibrations in Floating Offshore Wind Turbines [6,8,30]. Therefore, the constructed model of the suggested hybrid system puts emphasis on two movements: the fore-aft displacement at the top of the tower and the barge platform's pitch angle.

Additionally, this study delves into the vibration dynamics of the suggested hybrid structure, particularly in relation to waves. Notably, the effects of winds on the wind turbine were not taken into consideration to facilitate the establishment of a linear model and the design of an appropriate control approach [31]. Finally, the structural parameters configured in this research work are detailed in Table 2.

2.1. Modeling of the hybrid wind-wave FOWT system

In barge-based Floating Offshore Wind Turbines, the barge platform's pitch angle and the fore-aft translation of the tower are identified as the primary contributors to the bending moments of the tower [32–35]. Consequently, these two DoF have been carefully considered in the design of a simplified reduced-order model for the suggested floating hybrid wind-wave platform. The schematic representation of the proposed hybrid wind-wave floating platform concept is depicted in Fig. 2, adapted from [8,30].

The wind turbine tower is envisioned to be connected to the barge platform through a torsional spring and damper, functioning as the

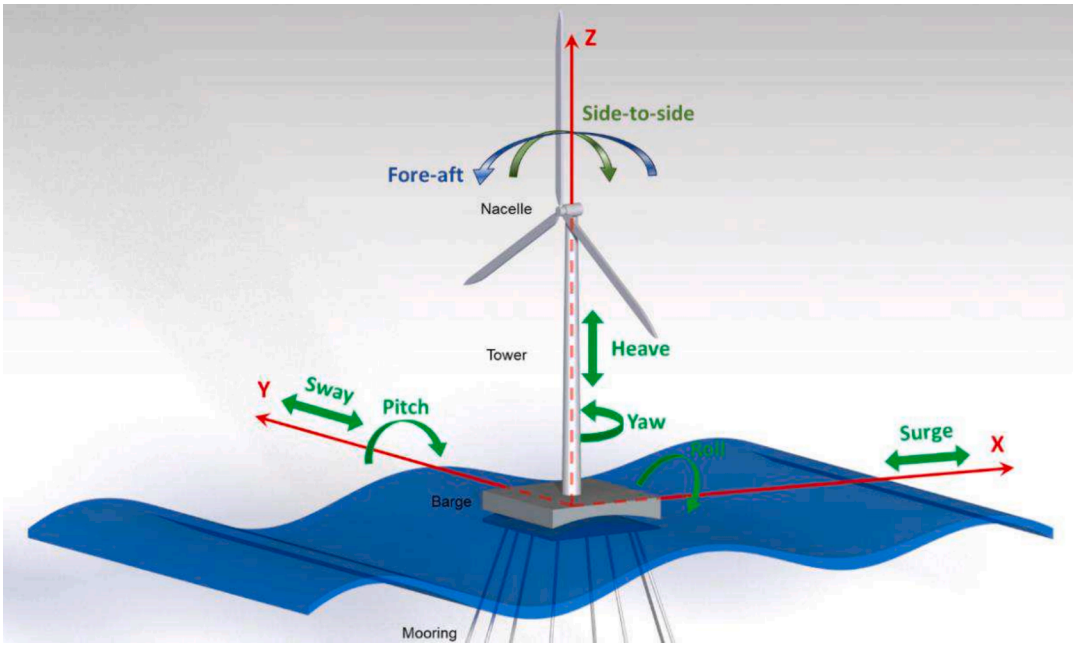

Fig. 1. Birdview and 6 DOFs of motions of a typical FOWT.

Table 1
NREL's 5 MW wind turbine and ITI Energy barge platform's parameters.

Wind Turbine		ITI Energy barge	
Feature	**Value**	**Feature**	**value**
Rating power	5 MW	Platform size	40 m x 40 m x10 m
Baseline control	Variable speed, collective pitch	Platform mass	5,452,000 kg
Cut-in, rated, cut-out wind speed	3 m/s, 11.4 m/s, 25 m/s	Anchor depth	150 *m*
Cut-in, rated rotor speed	6.9 rpm, 12.1 rpm	Number of mooring lines	8
Tower mass	347.460 kg	Line diameter	0.0809 *m*
Rotor diameter	126 *m*	Line mass	130.4 kg/m
Hub height	90 *m*		

Table 2
NREL's 5 MW wind turbine and ITI Energy barge's structural parameters.

Tower		ITI Energy barge	
Feature	**Value**	**Feature**	**value**
Stiffness	$k_t = 9.7990\ 10^9$ (N m rad^{-1})	Stiffness	$k_p = 1.4171\ 10^9$ (N m rad^{-1})
Damping coefficient	$d_t = 2.1032\ 10^7$ (N m s rad^{-1})	Damping coefficient	$d_p = 3.6374\ 10^7$ (N m s rad^{-1})
Inertia	$I_t = 1.8217\ 10^9$ (kg m^2)	Inertia	$I_p = 1.6945\ 10^9$ (kg m^2)

structural stiffness k_t and damping d_t. The mooring system's stiffness and the hydrostatic restoring torques exerted on the platform are simulated using a spring constant k_p, while the hydrodynamic damping, encompassing viscous and radiation effects of the waves, is depicted with a damping coefficient d_p, as illustrated in Fig. 2.

The integration of two OWCs into the barge platform aims to alleviate the platform's pitch angle and the tower's fore-aft translation within the system. In this study, emphasis has been placed on reducing oscillations along the ***x***-axis. Consequently, two identical OWCs have been incorporated, positioned at the front and back of the tower, equidistantly, to maintain symmetry along the ***x***-axis, as explained in Fig. 2. The specific characteristics of the OWCs are detailed in Table 3.

In a non-conservative system with n generalized DoF, the expression of Euler-Lagrange is formulated as follows:

$$\frac{d}{dt}\left(\frac{\partial L}{\partial \dot{q}_i}\right) - \frac{\partial L}{\partial q_i} = Q_i \quad (i = 1, 2, \cdots, n) \tag{1}$$

$$L = T - V \tag{2}$$

in this expression, T denotes the total kinetic energy, while V signifies the total potential energy. The symbol L represents the Lagrange operator, and Q_i corresponds to the generalized non-potential forces.

The combined kinetic and potential energies of the examined FOWT can be expressed as:

$$T = \frac{1}{2} I_t \dot{\theta}_t^2 + \frac{1}{2} I_p \dot{\theta}_p^2 \tag{3}$$

$$V = \frac{1}{2} k_t \left(\theta_t - \theta_p\right)^2 + \frac{1}{2} k_p \theta_p^2 + m_t g R_t \cos\theta_t - m_p g R_p \cos\theta_p \tag{4}$$

The generalized non-potential forces include the forces induced by wind and wave as:

$$\begin{cases} Q_{\theta_t} = -d_t\left(\dot{\theta}_t - \dot{\theta}_p\right) + M_{wind} \\ Q_{\theta_p} = -d_p\dot{\theta}_p + d_t\left(\dot{\theta}_t - \dot{\theta}_p\right) + M_{wave} - R_{owc1} f_{owc1} + R_{owc2} f_{owc2} \end{cases} \tag{5}$$

in this equation, θ denotes the rotation angle measured from the vertical z-axis, and k and d are the spring stiffness coefficient and damping coefficient. The variables m, I, and R signify the mass, inertia moment from the mass center (MC), and the distance from the MC to the base of the tower, respectively, with the subscripts p and t referring to platform and tower. M_{wind} and M_{wave} represent the bending torques resulting from wind and wave loads, while f_{owc1} and f_{owc2} denote the forces generated by the pressure in the OWC air chambers.

Utilizing small angles, as the pitch angle of floating structures typically does not surpass 10 degrees even in harsh wind and wave conditions, and given that OWC1 and OWC2 are equidistant to the tower base ($R_{OWC1} = R_{OWC2} = R_{OWC}$), the dynamic model can be defined by substituting equations (3), (4), and (5) into equations (1) and (2).

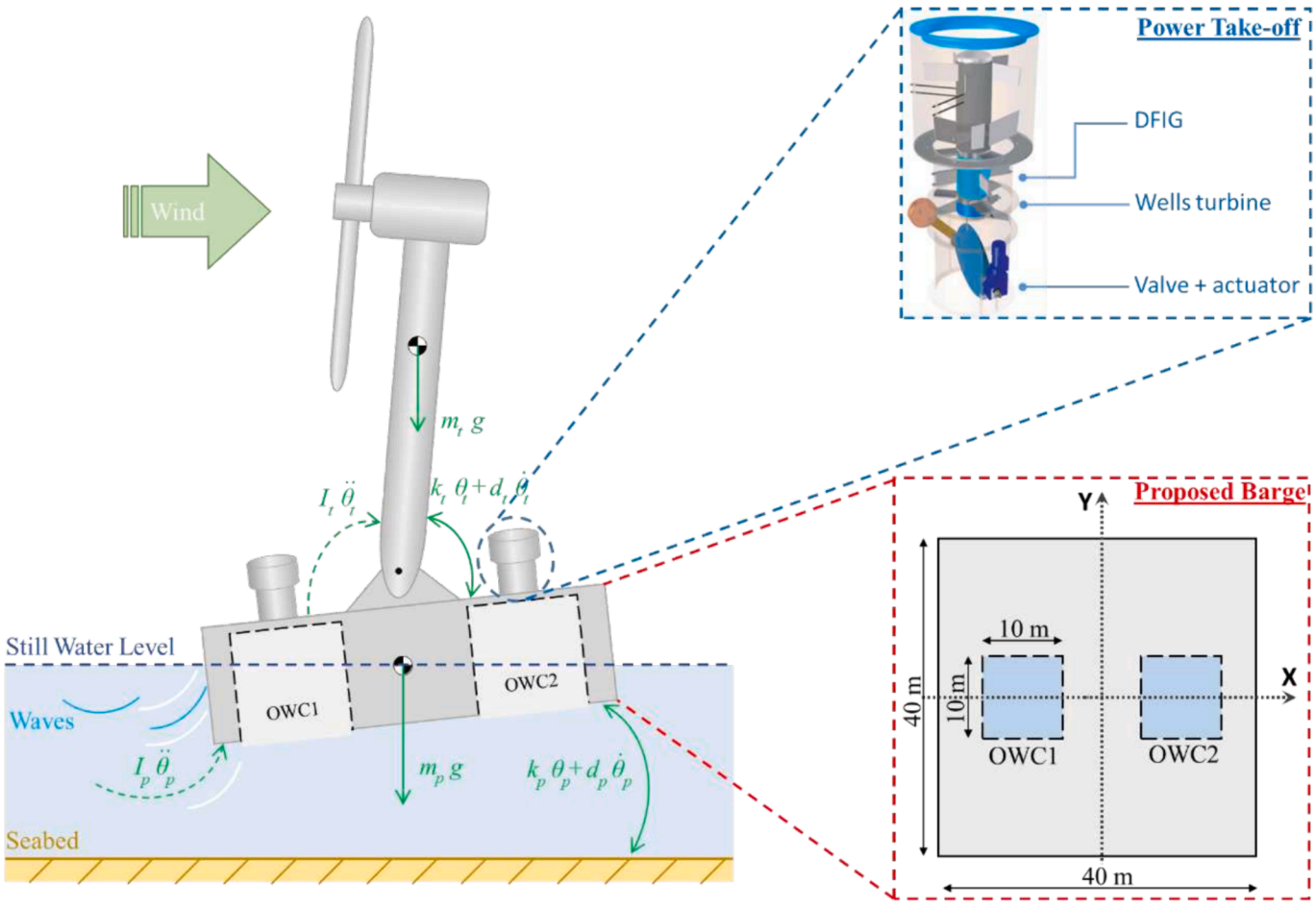

Fig. 2. Scheme of the novel hybrid wind-wave FOWT concept.

Table 3
Parameters of the capture chamber and Wells turbine of the considered OWCs.

Capture chamber		Wells turbine	
Feature	**Value**	**Feature**	**value**
Chamber's inner width	$w_c = 10\ m$	Blade number	$n = 5$
Chamber's inner length	$l_c = 10\ m$	Blade span	$b = 0.210\ m$
Chamber's inner height	$h_c = 9\ m$	Blade chord length	$l = 0.165\ m$
Water density	$\rho_c = 1029\ \mathrm{kg/m^3}$	Turbine mean radius	$r = 0.375\ m$
Atmospheric density	$\rho_a = 1.19\ \mathrm{kg/m^3}$	Cross-sectional area	$a = 0.4417\ \mathrm{m^2}$
Atmospheric pressure	$p_a = 101.325$ kPa		

$$\begin{cases} I_p\ddot{\theta}_p - k_t(\theta_t - \theta_p) + k_p\theta_p + m_p g R_p\theta_p = -d_p\dot{\theta}_p + \\ \qquad d_t\left(\dot{\theta}_t - \dot{\theta}_p\right) + M_{wave} - R_{owc}(f_{owc1} - f_{owc2}) \\ I_t\ddot{\theta}_t + k_t(\theta_t - \theta_p) - m_t g R_t\theta_t = -d_t\left(\dot{\theta}_t - \dot{\theta}_p\right) + M_{wind} \end{cases} \tag{6}$$

Let the M, D and K be the inertia, damping and stiffness matrices, respectively:

$$X = \begin{bmatrix}\theta_p \\ \theta_t\end{bmatrix},\ M = \begin{bmatrix}I_p & 0 \\ 0 & I_t\end{bmatrix},\ D = \begin{bmatrix}d_p + d_t & -d_t \\ -d_t & d_t\end{bmatrix},$$
$$K = \begin{bmatrix}k_p + k_t + m_p g R_p & -k_t \\ -k_t & k_t - m_t g R_t\end{bmatrix}$$

Thus, the system's equations of (6) can be rewritten as:

$$M\ddot{X} + D\dot{X} + KX = EM_{ext} + RF \tag{7}$$

$$M_{ext} = \begin{bmatrix}M_{wind} \\ M_{wave}\end{bmatrix},\quad F = \begin{bmatrix}f_{OWC1} - f_{OWC2} \\ 0\end{bmatrix},$$
$$E = \begin{bmatrix}0 & 1 \\ 1 & 0\end{bmatrix},\quad and\ R = \begin{bmatrix}-R_{OWC} & 0 \\ 0 & 0\end{bmatrix}$$

Equation (7) can be further arrange to a state-space model as follows:

$$\dot{X}_m = A_m X_m + B_m F + B_{ext} M_{ext} \tag{8}$$

$$X_m = \begin{bmatrix}X \\ \dot{X}\end{bmatrix},\ A_m = \begin{bmatrix}0 & I \\ -M^{-1}K & -M^{-1}D\end{bmatrix},$$
$$B_m = \begin{bmatrix}0 \\ M^{-1}R\end{bmatrix},\quad and\quad B_{ext} = \begin{bmatrix}0 \\ M^{-1}E\end{bmatrix}$$

Winds and waves interact with the floating system in the complex aero-elastic and hydro-elastic manner. Furthermore, wind- and wave-induced structural responses possess inherent connection [35].

For linear modeling, the wind and wave loads M_{wind} and M_{wave} were presumed to be linearly attained wind speed $V_{wind}(t)$ and the wave height $Z(t)$, therefore, M_{wind} and M_{wave} have been modeled as first-order functions [35]:

$$\dot{M}_{wind}(t) = -\alpha_{wind} M_{wind}(t) + \beta_{wind}\, V_{wind}(t) \tag{9}$$

$$\dot{M}_{wave}(t) = -\alpha_{wave} M_{wave}(t) + \beta_{wave}\, Z(t) \tag{10}$$

Using equations (9) and (10) in equation (8) the described system can be written as:

$$\dot{X} = AX + BU + B_w W \tag{11}$$

$$X = \begin{bmatrix} X_m \\ M_{wind} \\ M_{wave} \end{bmatrix},\ A = \begin{bmatrix} A_m & B_{ext} \\ 0 & \alpha \end{bmatrix},\ B = \begin{bmatrix} B_m \\ 0 \end{bmatrix},\ B_w = \begin{bmatrix} 0 \\ \beta \end{bmatrix},$$
$$U = \begin{bmatrix} F \\ 0 \end{bmatrix},\ W = \begin{bmatrix} V_{wind}(t) \\ Z(t) \end{bmatrix}$$

$$\alpha = \begin{bmatrix} \alpha_{wind} & 0 \\ 0 & \alpha_{wave} \end{bmatrix},\quad and\quad \beta = \begin{bmatrix} \beta_{wind} & 0 \\ 0 & \beta_{wave} \end{bmatrix}$$

In conclusion, the platform pitch angle and tower fore-aft translation are attained:

$$Y = CX \tag{12}$$

where $Y = \begin{bmatrix} Pitch \\ Fore-aft \end{bmatrix}$ and $C = \begin{bmatrix} 1 & 0 & 0 & 0 & 0 & 0 \\ -H_T & H_T & 0 & 0 & 0 & 0 \end{bmatrix}$.

2.2. Counteracting forces of OWCs

Assuming that the free-surface of the oscillating water inside the air chamber functions akin to a piston, enabling the consideration of uniform pressure. Consequently, the oscillating forces can be characterized by [34,36]:

$$f_{OWCi} = -p_i(t)\, S \qquad (i = 1,2) \tag{13}$$

here $p_i(t)$ is the pressure and S is the inner free-surface, $i = 1,2$ refers to OWC1 or OWC2.

Assuming the air within the air chamber behaves as an ideal gas, and considering the chamber to be adiabatic with transformations occurring slowly enough to be deemed reversible, the processes can be considered isentropic. As a result, the equation for air density may be formulated as:

$$\rho_i(t) = \rho_a \left(\frac{p_i(t)}{p_a}\right)^{\frac{1}{\gamma}} \qquad (i = 1,2) \tag{14}$$

in this context, p_a denotes atmospheric pressure, ρ_a signifies density, and γ denotes the specific heat ratio of air.

The earlier isentropic equation can be linearized to achieve:

$$\rho_i(t) = \rho_a \left(\frac{p_i(t)}{p_a \gamma}\right) \qquad (i = 1,2) \tag{15}$$

$$\dot{\rho}_i(t) = \frac{\rho_a}{p_a \gamma} \dot{p}_i(t) \qquad (i = 1,2) \tag{16}$$

Utilizing equations (15) and (16), it's possible de define the inner air's mass flowrate of the chamber may be expressed as:

$$\dot{m}_i(t) = \frac{d}{dt}(\rho_i(t)\ V_{OWCi}(t)\ ) = \frac{\rho_a V_0}{p_a \gamma} \dot{p}_i(t) + \rho_a\ \dot{V}_{OWCi}(t) \tag{17}$$

in this context, V_0 represents the chamber's undisturbed air volume, while $V_{OWC}(t)$ denotes the air volume.

The volume of the air is contingent on the shape of the chamber and can, therefore, be expressed as:

$$V_{OWCi}(t) = V_0 - S\, Z_1(t) \tag{18}$$

here $S = l_c.w_c$ is the chamber's inner free surface and Z_1 is the vertical translation of the piston-like water surface, rising in the ascending direction.

Henceforth, the inner pressure of the chamber changes in accordance to the air volume and the mass flowrate:

$$\dot{p}_i(t) = \frac{p_a \gamma}{\rho_a V_0}\ \dot{m}_i(t) - \frac{p_a \gamma}{V_0}\ \dot{V}_i(t) \qquad (i = 1,2) \tag{19}$$

Given that the OWCs are equipped with a Wells turbine, the formulas for its turbomachinery are taken into account. Consequently, the dimensionless flow coefficient can be articulated as:

$$\Phi = \frac{\dot{m}}{\rho_a\ \omega\ r^3} \tag{20}$$

in this equation, r represents the radius, and ω denotes the rotational velocity.

The flow coefficient relative to the Wells-type turbine can be expressed with the use of the axial velocity of air as:

$$\Phi = \frac{v_x}{r\ \omega} \tag{21}$$

in this context, v_x represents the axial speed of air passing through the turbine.

The volume flow rate may be expressed using the axial speed as:

$$Q = \frac{dV}{dt} = a\ v_x \tag{22}$$

in this equation, a represents the cross-sectional area of the Wells turbine.

By substituting equations (20) to (22) into equation (23), the pressure can be determined as a function of the airflow velocity:

$$\dot{p}_i(t) = \frac{p_a \gamma}{V_0} r^2\ v_{xi}(t) - \frac{p_a \gamma}{V_0}\ a\ v_{xi}(t) \qquad (i = 1,2) \tag{23}$$

3. PSODI-ANFIS airflow control strategy

The integration of OWCs is designed to generate forces resulting from the pressures confined within the capture chambers. These forces serve to counteract certain hydrodynamic forces. As the OWCs are positioned on opposite sides of the tower within the barge platform, they exert opposing moments. To capture air within the chambers during wave crests and generate pressure, the air valves located at the top must be closed. Conversely, to release air and decompress the chamber during wave troughs, the air valves should be opened. Given that wave crests and troughs progressively pass the barge platform, each valve needs to be gradually opened and closed. Therefore, this paper suggests an adaptive neuro-fuzzy inference system for airflow control to effectively manage the valves. The proposed ANFIS for airflow control relies on the platform pitch angle θ_p, as depicted in Fig. 3.

The input to the OWC-FOWT model is the wave height $Z(t)$, which can be acquired either through a wave height sensor positioned at the center of the barge or by utilizing an Acoustic Doppler Current Profiler affixed beneath the platform. The model's outputs are the platform pitch angle θ_p and the tower top fore-aft displacement x_t, both measurable using two accelerometers positioned at the top and bottom of the tower [34].

The proposed airflow control system utilizes an ANFIS to effectively manage the opening and closing of air valves based on the pitch angle θ_p, as illustrated in Fig. 3. The ANFIS controller takes the platform pitch angle error and its derivative e and $\dot{e}$ as inputs, producing the control

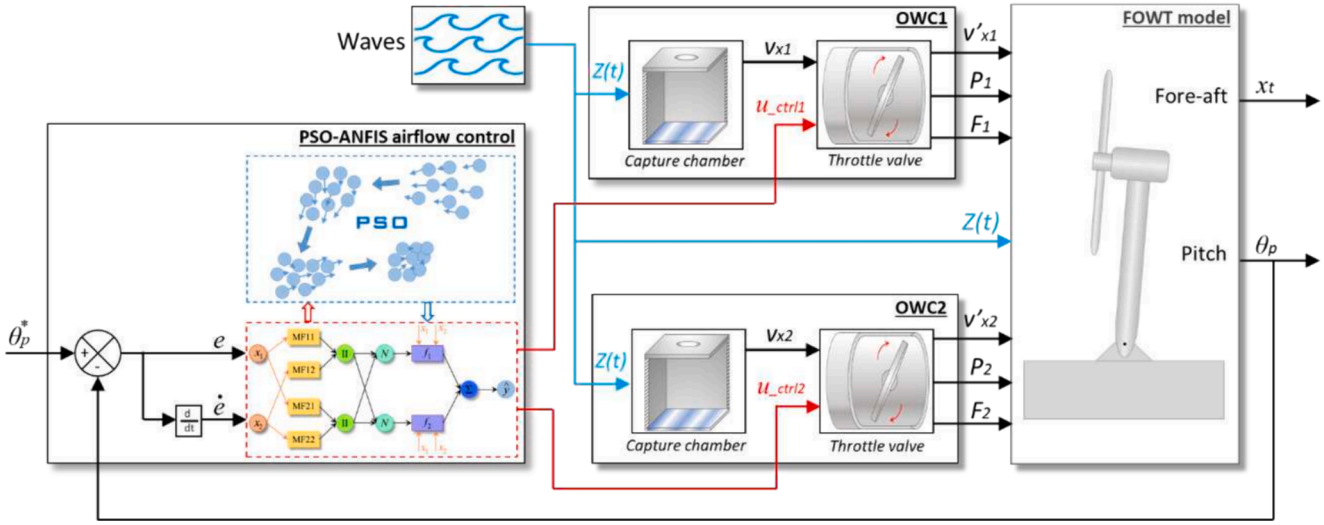

Fig. 3. Diagram of the proposed PSODI-ANFIS airflow control for the OWC-FOWT stabilization.

signals for the air valves, namely U_{ctrl1} and U_{ctrl2}, as outputs. As waves oscillate, the valves' opening and closing regulate the release or trapping of air, inducing compression or decompression within the chambers. Consequently, forces are generated in the chambers to counteract the hydrodynamic forces acting on the barge platform.

3.1. ANFIS model overview

The ANFIS technique was initially introduced by Jang in 1992 [37]. Since then, it has found widespread application as an optimization method for addressing complex and non-linear problems [38]-[39]. This hybrid system combines the capacity to make fuzzy logic decisions with the computational capability of neural networks, providing a sophisticated and advanced approach for modeling and estimation. The system leverages the trainability of neural networks and the robust decision-making capability of fuzzy systems, effectively addressing both uncertain and certain conditions.

3.1.1. Background and mathematical description

In a fundamental sense, ANFIS employs Artificial Neural Networks

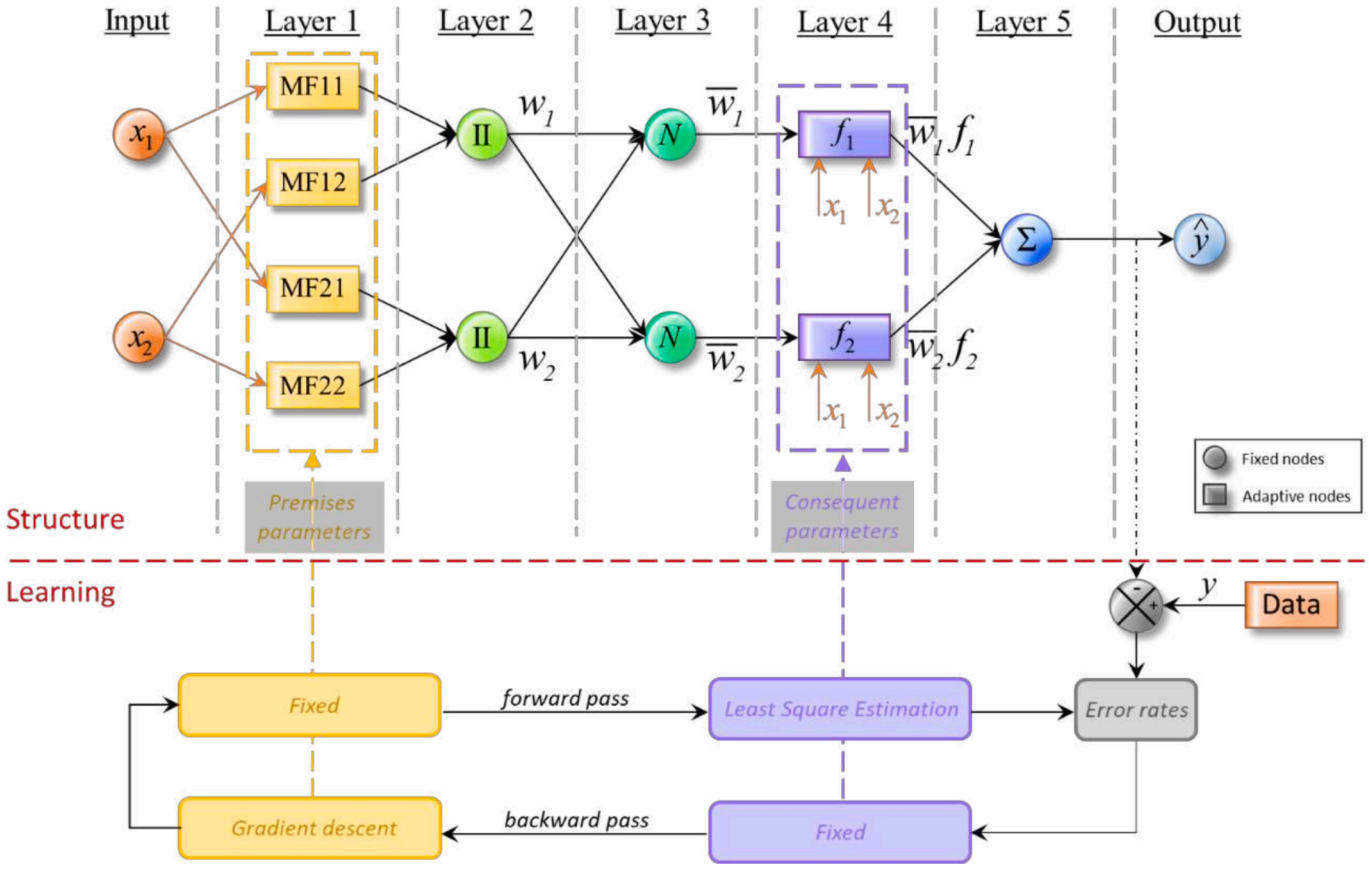

Fig. 4. Block diagram of an adaptive neuro-fuzzy inference system design.

(ANN) to enhance the values of Fuzzy Inference System (FIS) membership functions (MFs). This enhancement is achieved through a learning process utilizing two methods: Least Square Estimation (LSE) and Back-Propagation (BP) gradient descent. Fig. 4 depicts the structure of an ANFIS model, utilizing a Sugeno-type fuzzy inference system. The adaptive nodes in Layer 1 contribute to optimization, and in terms of precision, ANFIS results are more accurate compared to those obtained from a basic fuzzy system [40].

The ANFIS structure consists of an input layer, five hidden layers and the output layer as described in the block diagram of Fig. 4. In ANFIS structure, the number of membership functions must be equal to the number of rules and different rules cannot incorporate the same output membership function. The ANFIS rules are a set of IF-THEN rules defined as:

$$\begin{aligned} &Rule\ \ i: \quad \textbf{\textit{IF}}\ \ x_1\ is\ A_i\ and\ x_2\ is\ B_i \\ &\quad\ \ \textbf{\textit{THEN}}\quad f_i = p_i x_1 + q_i x_2 + r_i \end{aligned} \tag{24}$$

where f_i is first-order polynomial function, p_i, q_i and r_i are the design parameters determined during the training process.

Layer 1: It's known as the Fuzzifying layer where each neuron is an adaptive node consisting of premise parameters. The outcomes of layer 1 represent the fuzzy membership grades of the inputs.

Layer 2: Referred to as the Implication layer with fixed nodes, this layer incorporates fuzzy operators and employs the AND operator to fuzzify the inputs. The inputs, denoted by Π, act as simple multipliers.

Layer 3: Referred to as the Normalizing layer, this layer calculates the normalized firing strengths based on the outputs of layer 3. Each node in this layer represents a fixed rule labeled *N*.

Layer 4: Referred to as the Defuzzifying layer, each neuron in this layer is also adaptive, incorporating consequence parameters. The output of each node in this layer is the product of the normalized firing strength and a first-order polynomial.

Layer 5: Known as the Combining layer and it contains a single neuron. The single node in layer 5, labeled Σ, calculates the overall ANFIS output from the sum of the node inputs.

The design of the ANFIS model comprises two phases: construction and training. During the construction phase, the number and type of Membership Functions (MFs) are specified. Constructing the ANFIS model involves dividing the input/output data into rule patches to acquire the premise parameters. Various methods, such as Grid Partitioning (GP), Subtractive Clustering (SC), and FCM [41], can be employed for this purpose. The objective is to obtain a concise set of fuzzy rules.

In the training phase, the initial step involves generating training data pairs to train an ANFIS model. These data pairs include the ANFIS model inputs paired with their corresponding outputs. The learning process allows the membership function parameters to adapt, and the adjustment of consequent parameters is facilitated through supervised learning using the input/output dataset provided as training data to the model. Various learning techniques, including a hybrid learning algorithm that combines the LSE method and the Gradient Descent (GD) method, can be employed for this purpose.

ANFIS with FCM clustering will be applied, where the FCM is used to systematically create the fuzzy MFs and fuzzy rule base for ANFIS.

3.1.2. FCM clustering algorithm

In data clustering, clustering algorithms partition a given dataset $\mathbf{X}=\{x_1,\ldots,x_j,\ldots,x_n\}$ into c cluster groups $\mathbf{C}=\{c_1, \ldots, c_i, \ldots, c_c\}$with different cluster center $\mathbf{V}=\{v_1, \ldots, v_i, \ldots, v_c\}$. Data sets with the same characteristics belong to the same clusters, and non-similar data sets to different clusters. Hence, a partition matrix $\boldsymbol{U}$ is obtained consisting of membership degree μ_{ij} of data object x_j to cluster c_i. The FCM clustering is a non-monitoring clustering technique and its flexibility allows it to handle all data sizes as studied by T.C. Havens et *al.* in [42].

The positions of the cluster centers is measured using numerous types of distance metrics, such as the Manhattan distance, the Mahalanobis distance, or the cosine similarity [43]. The choice of distance metric depends on the nature and scale of the data, and the preferred similarity/dissimilarity definition between data points and clusters. However, the most common distance metric used is the Euclidean distance.

The Euclidean distance of data object x_j to cluster c_i with a centroid v_i maybe defined as:

$$d_{ij} = \sum_{i}^{c} \sum_{j}^{n} \left\| x_j - v_i \right\|^2 \tag{25}$$

where $i = 1,\ldots,c,$ with c is the number of cluster groups and $j = 1,\ldots,n$ with n is the number of data.

The i^{th} cluster centers v_i are updated using the following expression:

$$v_{ij} = \sum_{j=1}^{n} \left[\mu_{ij}\right]^m x_i \Big/ \sum_{j=1}^{n} \left[\mu_{ij}\right]^m \tag{26}$$

where m is the fuzzifier parameter that defines the level of cluster fuzziness and is a real number ($1 \leq m < \infty$) [44]. It is also known as the weighting exponent or fuzziness parameter.

The partition matrix $U(x)$ is updated through the fuzzy membership degree μ_{ij} of data x_j to cluster C_i iteratively, expressed as:

$$\begin{aligned} \boldsymbol{U}(\boldsymbol{X}, \boldsymbol{V}) &= \left[\mu_{ij}\right]_{c\times n} = \left[d_{ij}^{\frac{2}{m-1}} \Big/ \sum_{k=1}^{c} d_{kj}^{\frac{2}{m-1}} \right]^{-1} \\ &= \left[\left\| x_j - v_i \right\|^{\frac{2}{m-1}} \Big/ \sum_{k=1}^{c} \left\| x_k - v_i \right\|^{\frac{2}{m-1}} \right]^{-1} \end{aligned} \tag{27}$$

The FCM clustering algorithm aims to update each cluster center point v_{ij} and its corresponding membership degrees μ_{ij} iteratively by minimizing the objective function J that is defined as:

$$J = \sum_{i=1}^{c} \sum_{j=1}^{n} \mu_{ij}^m \left\| x_i - v_i \right\|^2 \tag{28}$$

The objective function J will continue minimizing until the positions of the cluster centers will not change or the difference of objective function J values between two iterations is within a threshold ε.

The ANFIS model development using FCM clustering algorithm is explained through the flowchart of Fig. 5.

3.2. ANFIS-PSODI model

The Particle Swarm Optimization is an evolutionary computation method first introduced in 1995 by J. Kennedy and R.C. Eberhart [45]. This sophisticated global optimization method draws inspiration from the swarming behavior observed in biological populations, such as bird flocks and fish schools [46]–[47].

3.2.1. Particle swarm optimization with decreasing inertia

The canonical PSO algorithm employs a swarm of particles, consisting of n_p particles represented as $x^1, x^2, \ldots, x^{n_p}$, distributed randomly within a bounded initial search space, to explore a global solution for a generic optimization problem [47]. Each particle, serving as a potential solution, possesses a position and a speed given by $\boldsymbol{x}_k^i = \left(x_k^{i,1}, x_k^{i,2} \cdots x_k^{i,d}\right)^T$ and $\boldsymbol{v}_k^i = \left(v_k^{i,1}, v_k^{i,2} \cdots v_k^{i,d}\right)^T$ where $(i,k) \in [\![1, n_p]\!] \times [\![1, k_{max}]\!]$.

During the k^{th} iteration of the algorithm, the position of the i^{th} particle, $x^i \in R^d$, evolves according to the following update rules:

$$\boldsymbol{x}_{k+1}^i = \boldsymbol{x}_k^i + \boldsymbol{v}_{k+1}^i \tag{29}$$

$$\boldsymbol{v}_{k+1}^i = w\boldsymbol{v}_k^i + c_1 \boldsymbol{r}_{1,k}^i \left(\boldsymbol{p}_k^i - \boldsymbol{x}_k^i\right) + c_2 \boldsymbol{r}_{2,k}^i \left(\boldsymbol{p}_k^g - \boldsymbol{x}_k^i\right) \tag{30}$$

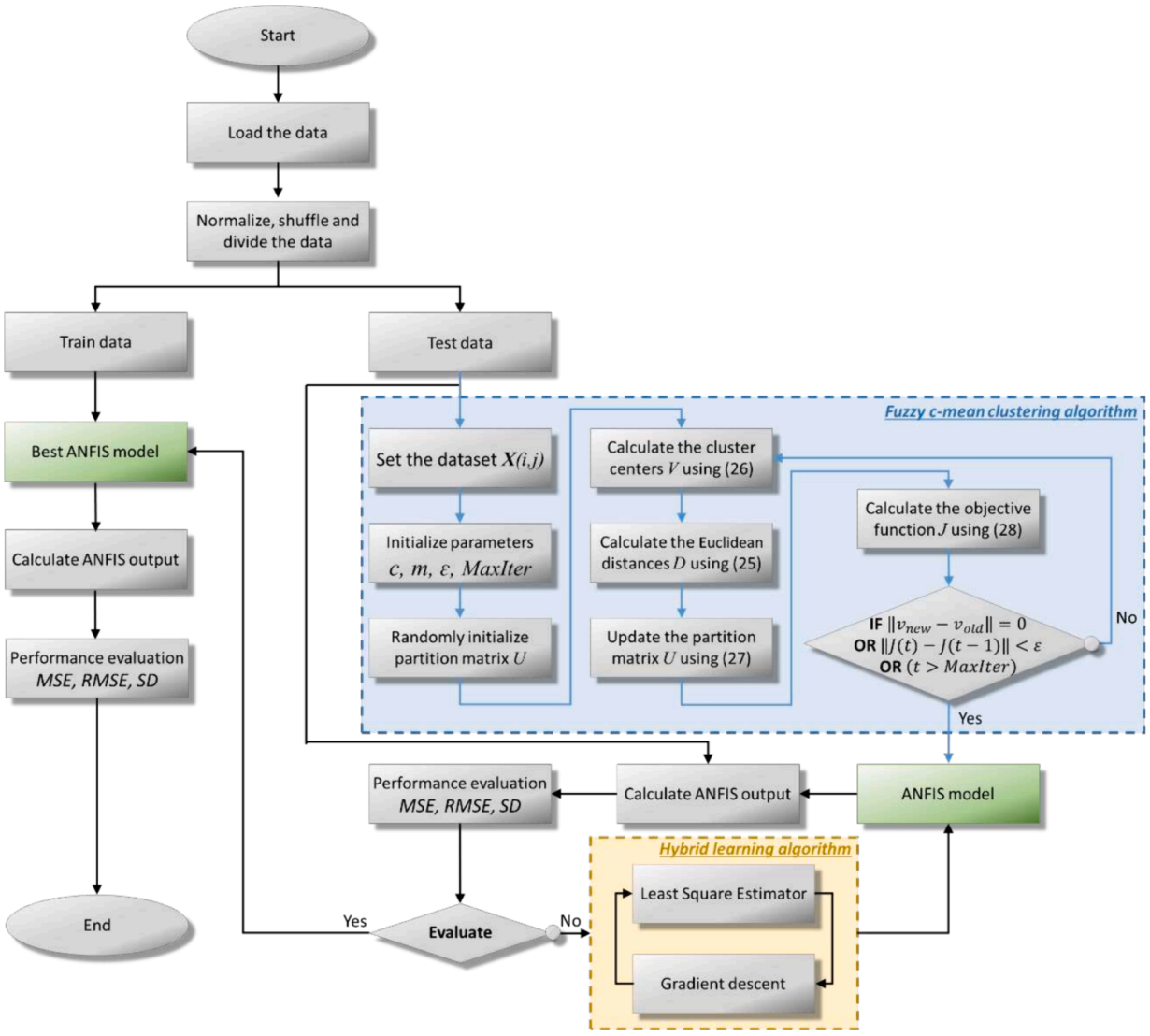

Fig. 5. Flowchart of ANFIS training and testing using Fuzzy c-mean clustering algorithm.

in this equation, w represents the inertia factor, c_1 is the cognitive acceleration coefficient, c_2 is the social acceleration coefficient, $r^i_{1,k}$ and $r^i_{2,k}$ are two random numbers uniformly distributed in the interval [0, 1], $\boldsymbol{p}^i_k$ is the best previously found position of the i^{th} particle, and $\boldsymbol{p}^g_k$ is the globally best-found position within the entire swarm at the current iteration k [47].

In the existing literature, the exploration and exploitation capabilities of the PSO algorithm can be enhanced by incorporating a linearly decreasing evolution mechanism for the inertia factor over iterations, as described in equation (39) in [46,47]. This variant of PSO is referred to as Particle Swarm Optimization with Decreasing Inertia (PSODI) algorithm.

$$w^i_{k+1} = \frac{w_{\max} - (w_{\max} - w_{\min})k}{k_{\max}} \tag{31}$$

in this equation, w_{max} and w_{min} represent the maximum and minimum inertia factors, typically assigned values of 0.9 and 0.4, respectively, as recommended by Eberhart and Shi [46]. The parameter k_{max} denotes the maximum number of iterations [47].

3.2.2. PSODI algorithm

The optimization problem for the airflow control strategy of the OWCs can be framed as a constrained and nonlinear optimization problem, denoted as (32), which will be addressed using the proposed PSODI algorithm:

$$\begin{cases} \text{minimize} \quad J(\boldsymbol{x}) \\ \boldsymbol{x} \in S \subseteq \mathbb{R}^d_+ \\ \textit{subject to}: \\ g_1(\boldsymbol{x}) = E_{ss} - E^{\max}_{ss} \\ g_2(\boldsymbol{x}) = t_r - t^{\max}_r \\ g_3(\boldsymbol{x}) = t_s - t^{\max}_s \end{cases} \tag{32}$$

here, J: $\mathbb{R}^d \to \mathbb{R}$ represents the cost function, where d is the dimension of the problem. $S = \{\boldsymbol{x} \in \mathbb{R}^d_+, \boldsymbol{x}_{\text{lower}} \le \boldsymbol{x} \le \boldsymbol{x}_{\text{upper}}\}$ denotes the bounded search space for the decision variables. The functions g_j: $\mathbb{R}^d \to \mathbb{R}$, ($j = 1, 2, 3$) represent the inequality constraints of the problem. The terms E_{ss}, t_r and t_s correspond to the criteria for steady-state error, rise time, and settling time, respectively. Additionally, E^{max}_{ss}, t^{max}_r and t^{max}_s signify the pre-specified maximum values for steady-state error, rise time, and settling time, respectively.

To handle the constraints of problem (32), various techniques have been suggested. One of these approaches involves applying penalties to

the cost function J. In this investigation, an external static penalty technique is taken into consideration and implemented in the following manner [47]:

$$\varphi(\boldsymbol{x}) = J(\boldsymbol{x}) + \sum_{j=1}^{n_{con}} \Lambda_j \max\left[0, \quad g_j(\boldsymbol{x})\right]^2 \tag{33}$$

here, J is the cost function, Λ_j represents scaling penalty parameters, and n_{con} is the number of constraints.

The development of ANFIS model using the FCM clustering algorithm and PSODI algorithm is explained through the flowchart of Fig. 6.

4. Results and discussion

This section will study two aspects of the results of the proposed PSODI-ANFIS. The first aspect is the PSODI-ANFIS training and its performance and the second aspect is the simulation of the PSODI-ANFIS airflow control in the hybrid OWC-FOWT platform.

4.1. PSODI-ANFIS training

The data used in this experiment, consists of a total of 10,357 samples. They samples has been normalized, shuffled and divided to 70 % for training (7250 samples) and 30 % for testing (3107 samples). The proposed PSODI-ANFIS will be compared to the standard ANFIS trained with FCM clustering. The parameters of the proposed PSODI-ANFIS are summarized in Table 4.

Table 4
Parameters of the proposed PSODI-ANFIS.

ANFIS parameters		PSODI parameters	
Number of inputs	2	Population size (n_p)	35
Number of outputs	1	Cognitive acceleration (C_1)	1
Partitioning method	Fuzzy c-mean	Social acceleration (C_2)	2
Input MF type	gaussmf	Minimum inertia factor (w_{min})	0.4
Output MF type	linear	Maximum inertia factor (w_{max})	0.9
And method	prod	Maximum iterations (k_{max})	500
Or method	probor		
Implication	min		
Aggregation	max		
Defuzzication	wtaver		

To evaluate the performance of the trained PSODI-ANFIS controller error based performance criteria has been computed. The error is between the target output y and the predicted output $\hat{y}$ hence, the error rates are defined by Error Mean (EM), Error Standard Deviation (ESD), Mean Square Error (MSE) and Root Mean Square Error (RMSE) as follow:

(continued on next page)

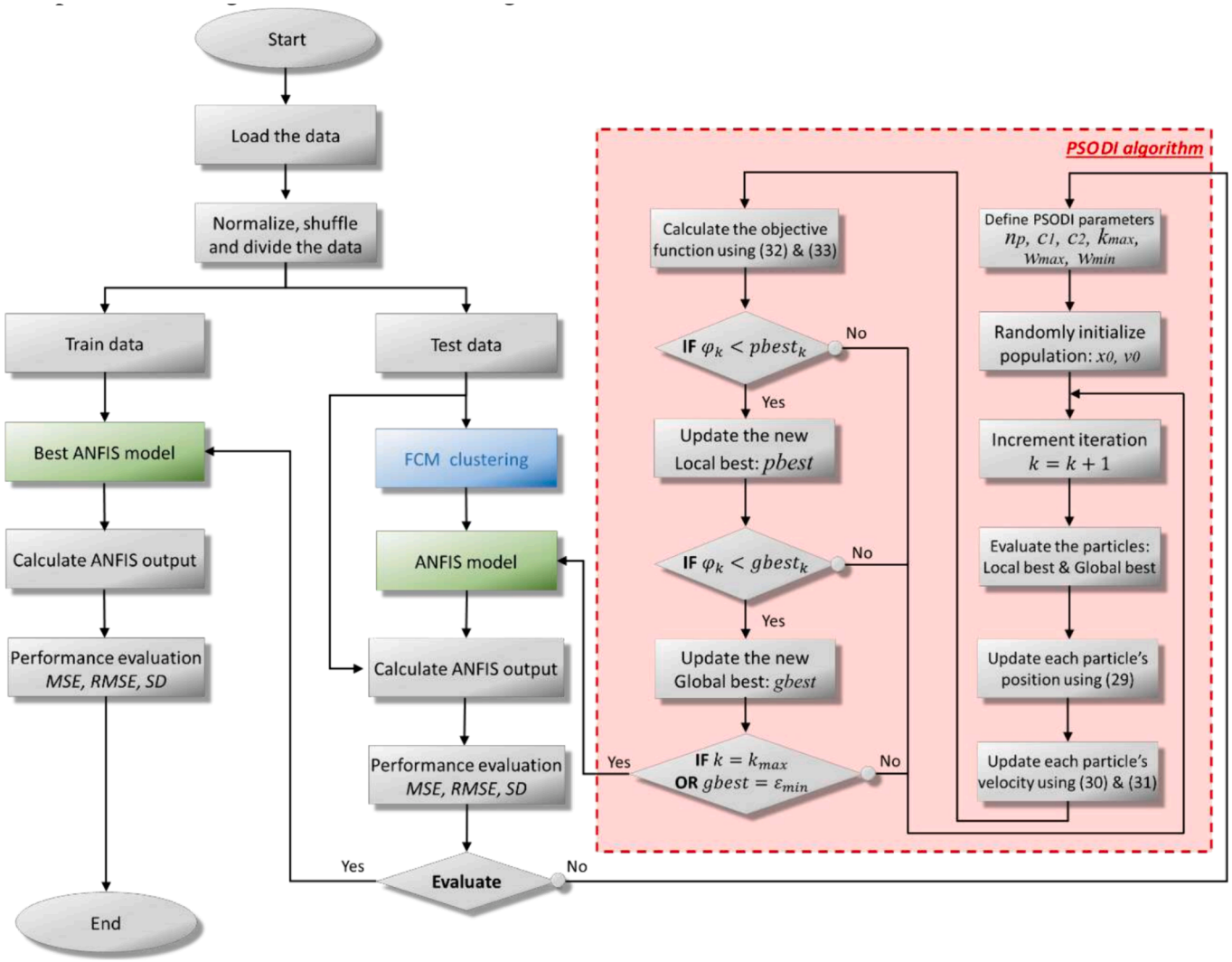

Fig. 6. Flowchart of ANFIS training and testing using PSODI algorithm.

(*continued*)

Error Mean: $EM = \frac{1}{n}\sum_{i=1}^{n}(y_i - \hat{y}_i)$ where n is the number of samples.	**Mean Square Error:** $MSE = \frac{1}{n}\sum_{i=1}^{n}(y_i - \hat{y}_i)^2$ where n is the number of samples.
Error Mean: $EM = \frac{1}{n}\sum_{i=1}^{n}(y_i - \hat{y}_i)$ where n is the number of samples.	**Mean Square Error:** $MSE = \frac{1}{n}\sum_{i=1}^{n}(y_i - \hat{y}_i)^2$ where n is the number of samples.
Error Standard Deviation: $ESD = \frac{\sigma}{\sqrt{n}} = \sqrt{\sum_{i=1}^{n}(\boldsymbol{y_i} - \bar{y})^2/(n-1)}/\sqrt{n}$ where σ is the standard deviation, $\boldsymbol{y_i}$ is the summation of the outputs up to the i^{th} value and $\bar{y}$ is the mean output.	**Root Mean Square Error:** $RMSE = \sqrt{\frac{1}{n}\sum_{i=1}^{n}(y_i - \hat{y}_i)^2}$ where n is the number of samples.

First, using the training data of Fig. 7.a. and Fig. 8.a. the obtained FCM-ANFIS and PSODI-ANFIS controller model yielded the training errors of Fig. 7.b. and Fig. 8.b.

After the training phase, testing data has been used to test the trained FCM-ANFIS and PSODI-ANFIS controller models. Testing data of Fig. 9.a. and Fig. 10.a. the obtained FCM-ANFIS and PSODI-ANFIS controller model yielded the testing errors of Fig. 9.b. and Fig. 10.b.

The obtained training errors of the FCM-ANFIS model in Fig. 7.b. are clearly higher than that of the PSODI-ANFIS controller shown in Fig. 8.b. The same can be observed in testing errors where the testing errors of the FCM-ANFIS model in Fig. 9.b. are clearly higher than that of the PSODI-ANFIS controller shown in Fig. 10.b.

The superiority of the PSODI-ANFIS controller over the FCM-ANFIS controller can be further confirmed by the error histograms illustrated in Figs. 11 and 12.

The training performance indicators of the trained ANFIS and PSODI-ANFIS models are presented in Table 5 summarizing the performance evaluation of the obtained errors in Figs. 7 to 12. As explained in Table 5, for the ANFIS model, the distribution of the error concentrates between -10^{-04} and 10^{-04} with 6580 of the samples representing 90 % of the data and a peak at $-1.85\ 10^{-06}$ with 5614 representing 77 % of the data during training. And during testing, the distribution of the error concentrates between -10^{-04} and 10^{-04} with 2816 of the samples representing 90 % of the data and a peak at $-3.53\ 10^{-06}$ with 2360 representing 76 % of the data.

On the other hand, for the PSODI-ANFIS model, the distribution of the error concentrates between $-3x10^{-16}$ and $3x10^{-16}$ with 7206 of the samples representing 99 % of the data and a peak at $-6.25\ 10^{-18}$ with 7206 representing 31 % of the data during training. And during testing, the distribution of the error concentrates between $-3x10^{-16}$ and $3x10^{-16}$ with 3077 of the samples representing 99 % of the data and a peak at $-6.45\ 10^{-06}$ with 979 representing 31 % of the data.

The performance analysis between the standard ANFIS trained with FCM clustering and the PSODI-ANFIS is based on the obtained error rates, which are summarized in Table 6. Both ANFIS models were compared to a Feed Forward Neural Network (FFNN) and Multi-Layer Perceptrons (MLP) for further analysis and understanding of the advantages of the proposed model. A simple FFNN (2x4x2) consisting of two neurons in the input layer, one hidden layer with four neurons and two neurons in the output layer has been considered. As for the MLP a (2x4x4x4x2) network has been considered consisting of two neurons in the input layer, three hidden layers with four neurons and two neurons in the output layer.

According to the error rates presented in Table 6, the MSE measures the overall fit of the model to the data. The MSE of the FFNN and MLP models offer a slightly higher MSE than that of the standard ANFIS this is due to the fact that ANFIS have the inherent capabilities of neural networks with the added capabilities of fuzzy logic systems. However, the lowest MSE is $7.4967\ 10^{-33}$ obtained with the PSODI-ANFIS model indicating superiority in terms of performance.

On the other hand, the RMSE measures the dispersion of errors of the model to the data. The RMSE of the FFNN and MLP models are slightly higher than that of the standard ANFIS. However, the lowest RMSE is $8.6583\ 10^{-17}$ obtained with the PSODI-ANFIS model indicating superiority in terms of prediction accuracy.

The performance of the PSODI to train the ANFIS architecture can be analyzed from the convergence curve of the algorithm during training, which is illustrated in Fig. 13.

The convergence curve shows that the PSODI managed to find a local

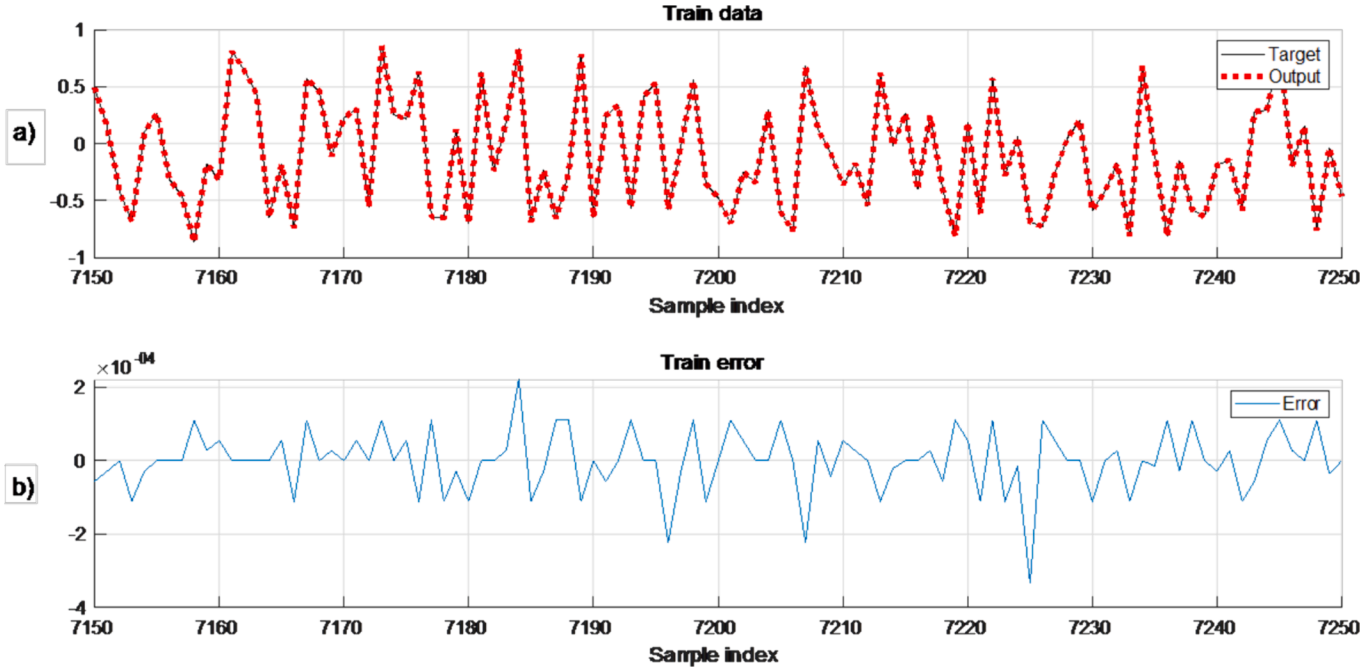

Fig. 7. Training data of ANFIS model. a) Target data and predicted output. b) Train error.

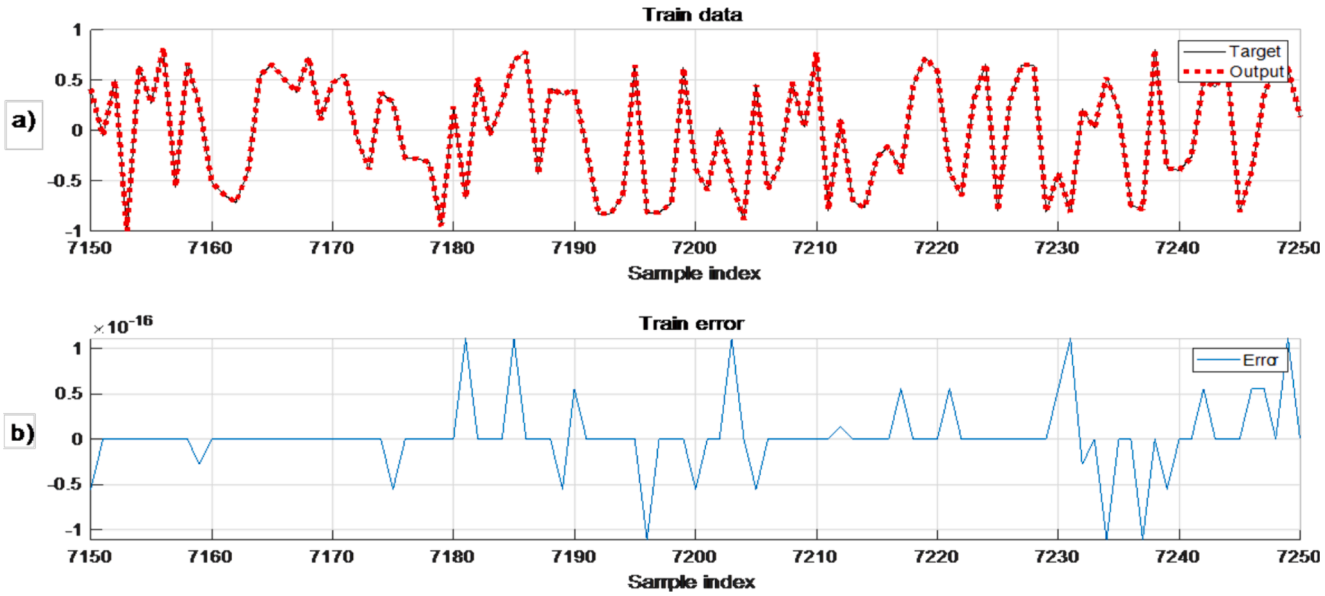

Fig. 8. Training data of PSODI-ANFIS model. a) Target data and predicted output. b) Train error.

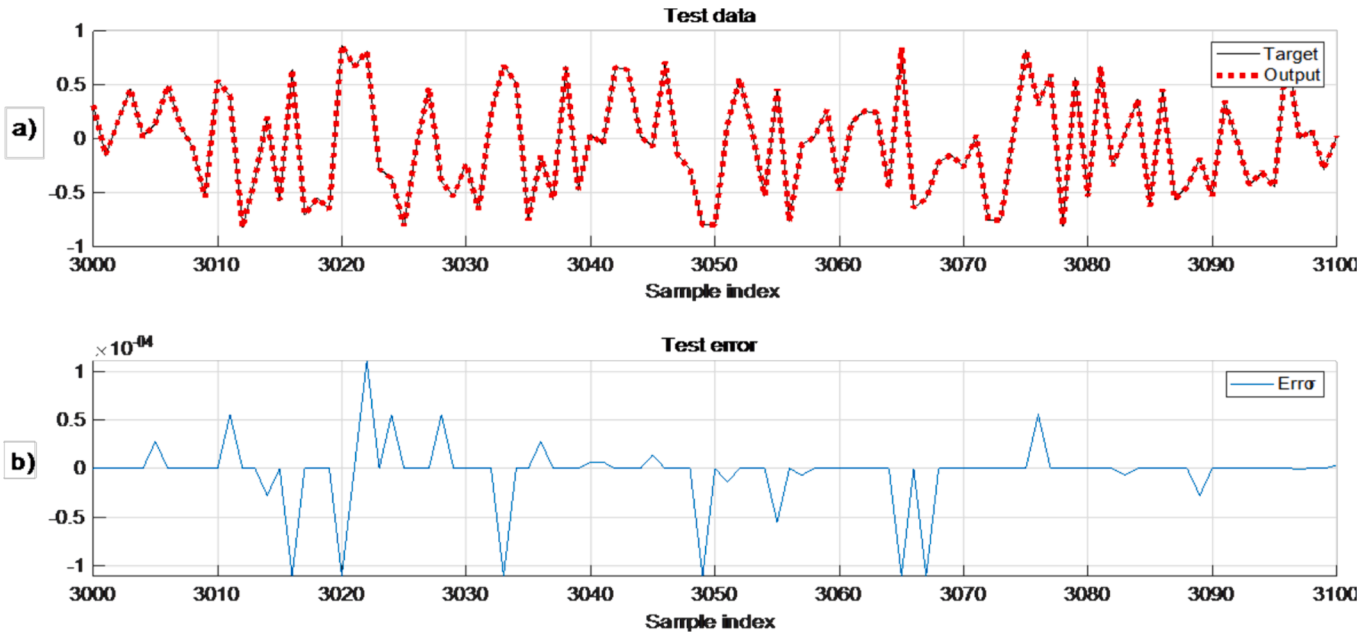

Fig. 9. Testing data of ANFIS model. a) Target data and predicted output. b) Test error.

region of interesting research space in the first iterations for RMSE around 8.85 10^{-17}. However, it managed to find the global solution after 224 iterations with a RMSE = 8.52 10^{-17}. Both the number of iteration and the value of the global solution demonstrate the speed, efficiency and precision of the PSODI to train the ANFIS model.

4.2. *PSODI-ANFIS control simulation of the OWC-FOWT*

To assess the structural response of the proposed hybrid Floating Offshore Wind Turbine with Oscillating Water Columns and evaluate the efficiency of the developed PSODI-ANFIS airflow control, a simulation was conducted utilizing the resonance frequency of the proposed hybrid OWC-FOWT concept [24]. Based on the Response Amplitude Operator (RAO) of the floating platform pitch depicted in Fig. 14, the resonance aligns with waves having a period of 11.6 s. Moreover, the results of the PSODI-ANFIS airflow control will be compared to those of a Fuzzy airflow control obtained in [23].

Using the resonance frequency, a wave input with an amplitude of 1 m and a period of 11.6 s has been introduced to the numerical model of the hybrid OWC-FOWT as shown in Fig. 15.

The airflow attained inside the air chambers of the first OWC1 and the second OWC2 is depicted in Fig. 16.a. and Fig. 16.b., respectively.

The three cases considered are the uncontrolled scenario, the scenario with Fuzzy airflow control, and the scenario with PSODI-ANFIS airflow control. It is evident that when control is active, the valves lead to a reduction in airflow speed, while the valves remain consistently open in the uncontrolled case (black curves). Nonetheless, there are discernible differences in airflow levels between the fuzzy-controlled and PSODI-ANFIS-controlled scenarios. Specifically, it is observed that the PSODI-ANFIS controller achieves a greater reduction in airflow

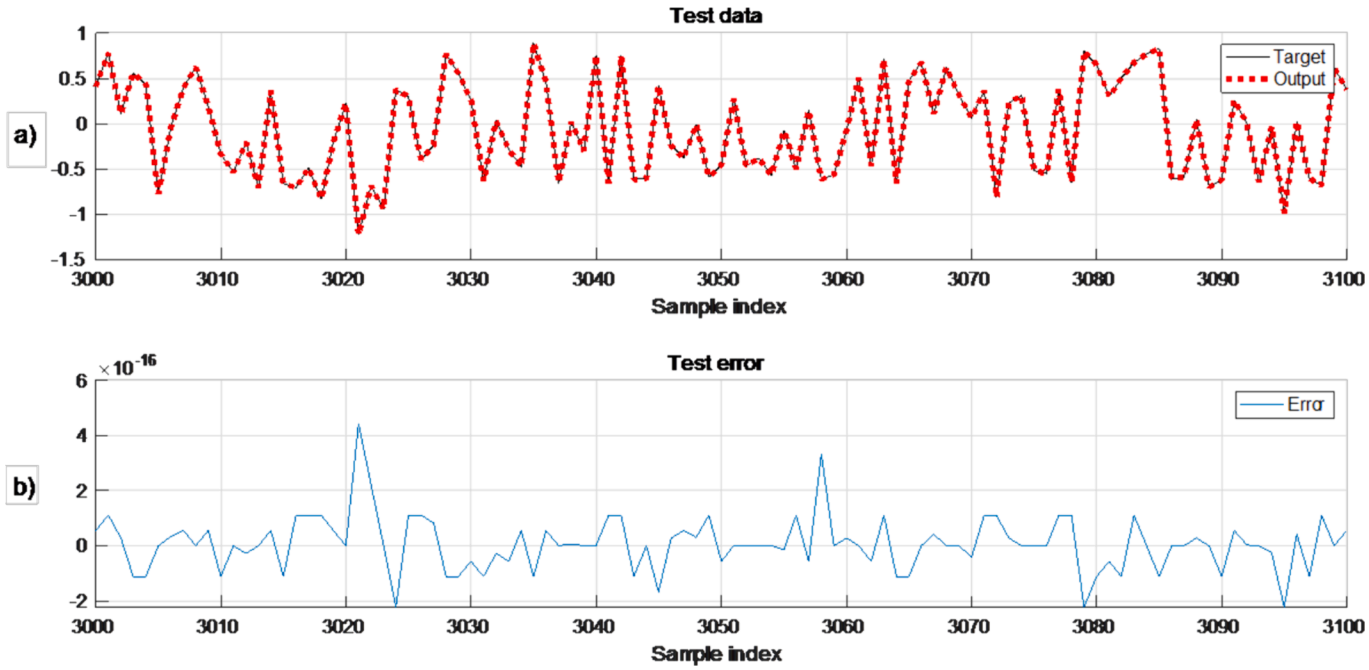

Fig. 10. Testing data of PSODI-ANFIS model. a) Target data and predicted output. b) Test error.

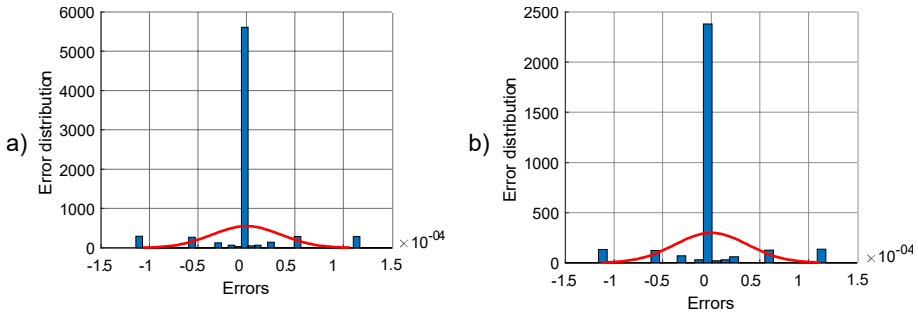

Fig. 11. Histogram of errors for ANFIS model a) Training errors. b) Testing errors.

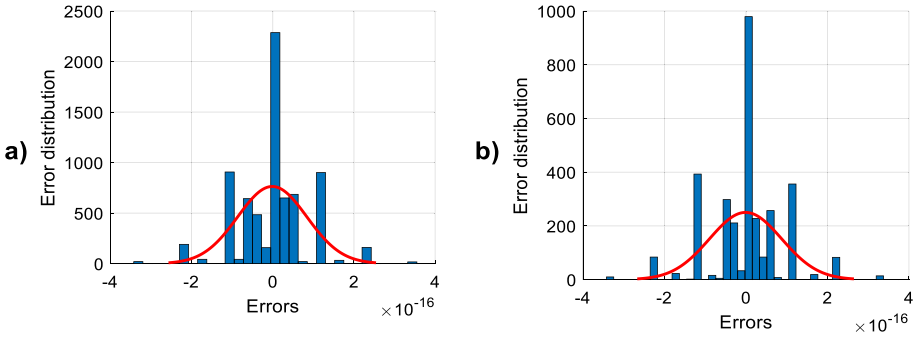

Fig. 12. Histogram of errors for PSODI-ANFIS model a) Training errors. b) Testing errors.

speed compared to the fuzzy controller.

The pressures generated in the capture chambers, derived from the airflow velocity of OWC1 and OWC2 as shown in Fig. 16, are presented in Fig. 17.a. and Fig. 17.b. for the uncontrolled FOWT, Fuzzy airflow control, and PSODI-ANFIS airflow control scenarios. The outcomes of the controlled air-valves are evident in the chamber pressure represented by the red and blue curves. Notably, due to the closure of the valves, the pressure is retained at a higher level compared to the uncontrolled FOWT (black curves), where it declines to the atmospheric pressure. Furthermore, the average pressure achieved with PSODI-ANFIS control exhibits higher values than that obtained with fuzzy control.

Subsequently, the pitch angle of the barge platform when using the Fuzzy airflow-controlled OWC-FOWT and the PSODI-ANFIS airflow-controlled OWC-FOWT is depicted in Fig. 18, and it is compared to the pitch angle of the standard barge-type FOWT. Referring to these results, both the Fuzzy and PSODI-ANFIS-controlled systems effectively regulate the valves based on the platform pitch, resulting in the notable reduction

Table 5
Training performance evaluation indicators.

Data	Indicators	Total	ANFIS		PSODI-ANFIS	
			Peak error (at −1.85 10^{-06})	|Error| 90 % between [-1, 1] 10^{04}	Peak error at **−6.45 10^{-18}**	|Error| 90 % between [-3, 3] 10^{16}
Training data		7250	5614	6580	2286	7206
Testing data		3107	2360	2816	979	3077

Table 6
Performances of the trained models.

Model	Analysis	EM	ESD	MSE	RMSE
FFNN	**Training**	−4.0661 10^{-05}	6.3712 10^{-04}	4.0648 10^{07}	6.3756 10^{04}
	Testing	−5.7943 10^{-05}	6.6507 10^{-04}	4.4744 10^{07}	6.6891 10^{04}
	All	−4.5846 10^{-05}	6.4550 10^{-04}	4.1856 10^{07}	6.4696 10^{04}
MLP	**Training**	−2.2434 10^{-05}	1.5086 10^{-04}	2.3113 10^{08}	1.5203 10^{04}
	Testing	−3.6742 10^{-05}	1.8215 10^{-04}	3.3577 10^{08}	1.8324 10^{04}
	All	−2.6726 10^{-05}	1.6025 10^{-04}	2.6047 10^{08}	1.6139 10^{04}
ANFIS	**Training**	−1.0100 10^{-06}	3.5602 10^{-05}	1.2706 10^{09}	3.5645 10^{05}
	Testing	−8.0611 10^{-05}	3.7403 10^{-05}	1.4045 10^{09}	3.7477 10^{05}
	All	−7.0742 10^{-04}	3.6811 10^{-05}	1.3671 10^{09}	3.6815 10^{05}
PSODI-ANFIS	**Training**	−1.2701 10^{-18}	8.5200 10^{-17}	7.2502 10^{33}	8.5148 10^{17}
	Testing	−1.0301 10^{-16}	8.8603 10^{-17}	7.8575 10^{33}	8.8643 10^{17}
	All	−1.4428 10^{-16}	8.2683 10^{-17}	**7.4967 10^{-33}**	**8.6583 10^{-17}**

in the platform pitch. Specifically, the pitch angle decreases from 8.304° in a standard barge to 3.470° in a Fuzzy-controlled OWC-based barge and further to 2.992° in a PSODI-ANFIS-controlled OWC-based barge.

The achieved tower top fore-aft displacement (TTD_{FA}) of the oscillating water column-based Floating Offshore Wind Turbine controlled by the Fuzzy and PSODI-ANFIS were compared to the TTD_{FA} of the standard Floating Offshore Wind Turbine, as illustrated in Fig. 19. Same as the pitch angle, it is evident that both the FOWT controlled with fuzzy and FOWT controlled with PSODI-ANFIS have effectively reduced the TTD_{FA} under resonant wave condition.

Specifically, in a standard FOWT the TTD_{FA} is 1.3913 m and decreases to 0.5881 m in the OWC-FOWT with the fuzzy control while it decreases further to 0.5002 m in the OWC-FOWT with the PSODI-ANFIS control.

The obtained results are summarized in Table 7. The Fuzzy-controlled OWC-based FOWT effectively reduces platform pitch vibrations by an average of 57 % and tower top fore-aft bending by an average of 58 %. In contrast, the PSODI-ANFIS controlled OWC-based FOWT demonstrates even greater efficacy, reducing platform pitch vibrations by an average of 63 % and tower top fore-aft bending by an average of 64 %.

5. Conclusions

In this research, a novel active structural control system has been created via the integration of two OWCs inside the structure of a barge platform of a FOWT. The primary objective is to enhance platform stability by mitigating both platform pitch and tower top fore-aft displacements. This innovative approach leverages counterforces generated by the air decompression within the air chambers of both OWCs to effectively reduce undesired platform pitching and tower top fore-aft displacement (TTD_{FA}).

To achieve this goal, a dynamic and reduced modeling of the proposed hybrid OWC-based FOWT has been formulated, with a specific focus on the DoFs related to the pitch angle and TTD_{FA}. The established mathematical representation incorporates pressures and forces generated by both integrated oscillating water columns to assess their impact on resisting hydrodynamic forces that influence platform stability. To regulate the OWCs and counteract undesired movements, a PSODI-ANFIS airflow control system has been implemented. This control mechanism dynamically adjusts the opening and closing of the valves in the integrated OWCs based on the platform's pitching, effectively managing the pressures within the capture chambers. The obtained results reveal significant improvements when comparing the proposed systems with the standard FOWT and the OWC-based FOWT with a fuzzy control, under various wave conditions. The OWC-based FOWT with a

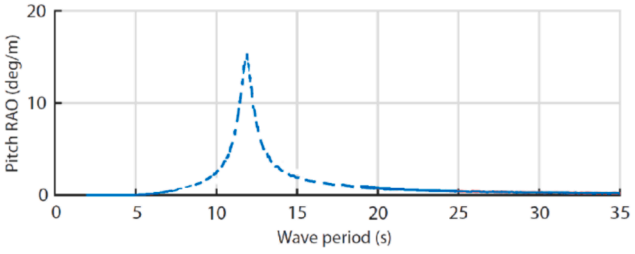

Fig. 14. Pitch RAO of the FOWT system.

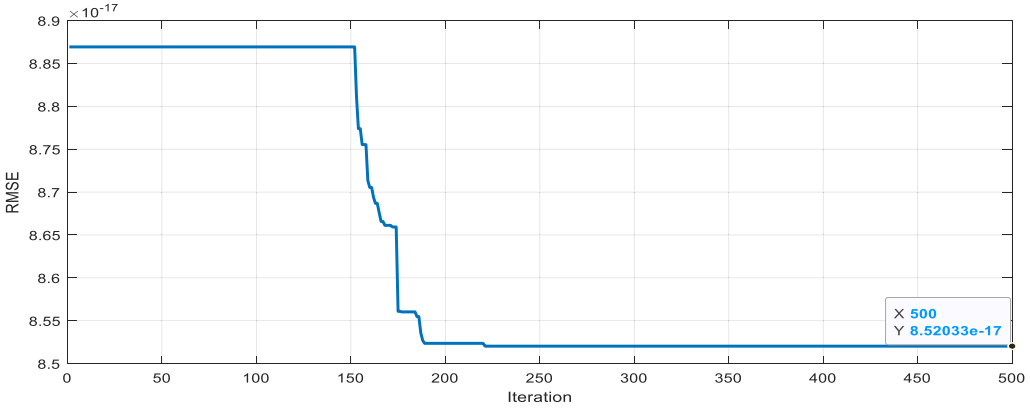

Fig. 13. Convergence curve of PSODI used on ANFIS training.

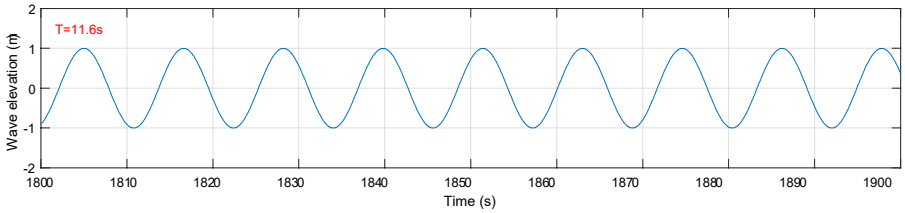

Fig. 15. Chosen wave input $Z(t)$ with the resonant wave period.

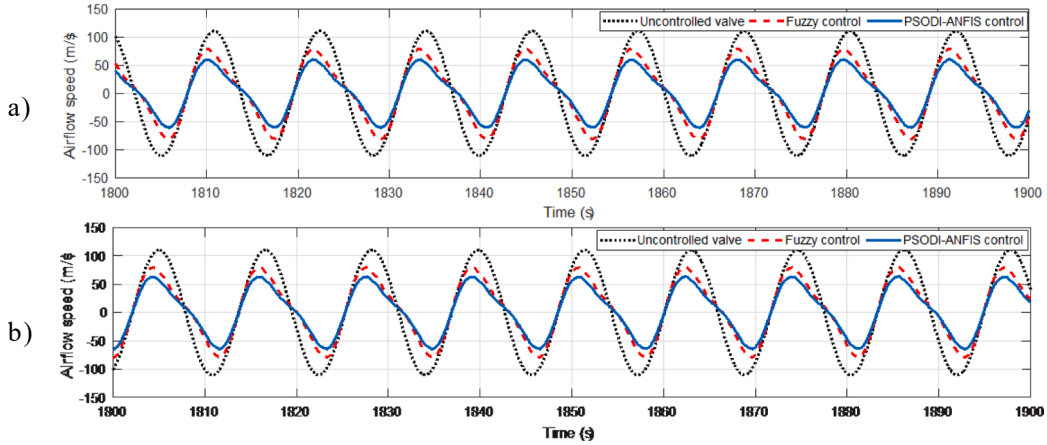

Fig. 16. Airflow speed inside the capture chambers (a) in OWC1 and (b) in OWC2.

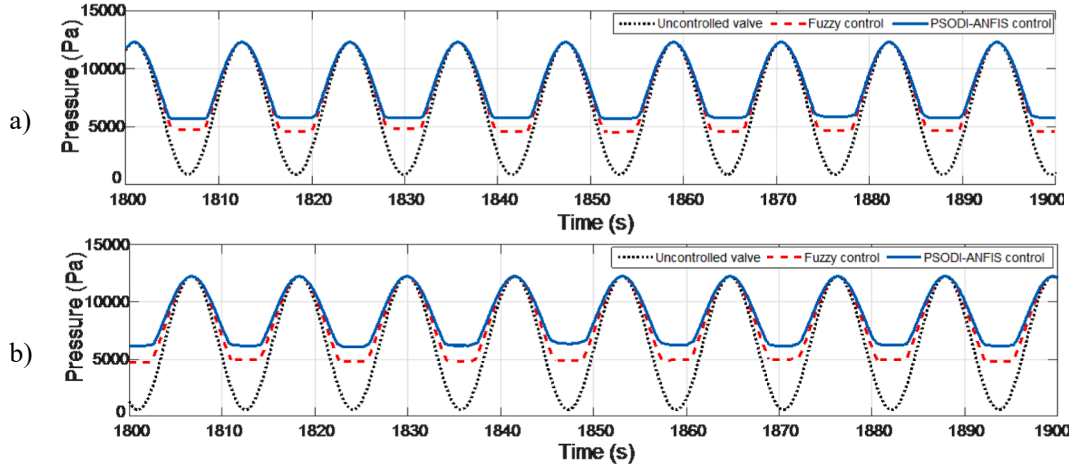

Fig. 17. Air pressure inside the capture chambers (a) in OWC1 and (b) in OWC2.

fuzzy control effectively reduces platform pitch vibrations by an average of 57 % and the TTD_{FA} by an average of 58 %. In contrast, the PSODI-ANFIS controlled OWC-based FOWT demonstrates even greater efficacy, reducing platform pitch vibrations by an average of 63 % and the TTD_{FA} by an average of 64 %. These outcomes underscore the superior performance of the PSODI-ANFIS control strategy in enhancing the stability of the offshore wind turbine system.

The positive outcomes obtained from the proposed control strategies can be extrapolated to address additional undesired oscillatory motions. By implementing additional pairs of OWCs in different directions, such as platform roll motion and tower top side-to-side displacement, the demonstrated control methods have the potential to effectively mitigate these motions. This extension of the control approach showcases the versatility and applicability of the proposed system for comprehensive stability enhancement in various operational scenarios. On the other hand, the limitations are attributed to the simplified linear model, which narrows the scope of the system's observed degrees of freedom, and the linearization of the isotropic equation, potentially decreasing the precision of pneumatic pressure calculations and, consequently, the induced forces from the OWC chambers.

Funding

This work was supported in part through grant IT1555-22 funded by the Basque Government, through grants PID2021-123543OBC21 and PID2021-123543OB-C22 funded by MICIU/AEI/https://doi.org/10.13039/501100011033 and by ERDF/EU and through the María Zambrano grant MAZAM22/15 funded by UPV-EHU/MIU/Next Generation, EU.

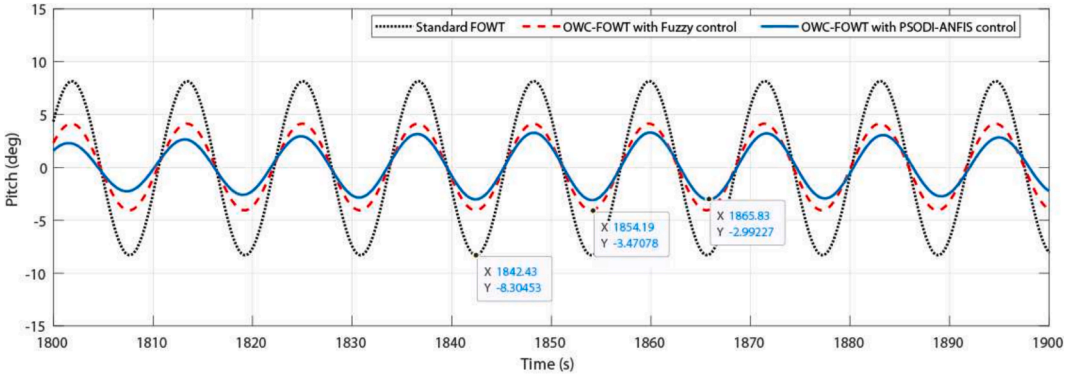

Fig. 18. Platform pitch for standard FOWT vs. Fuzzy-controlled OWC-FOWT and PSODI-ANFIS-controlled OWC-FOWT.

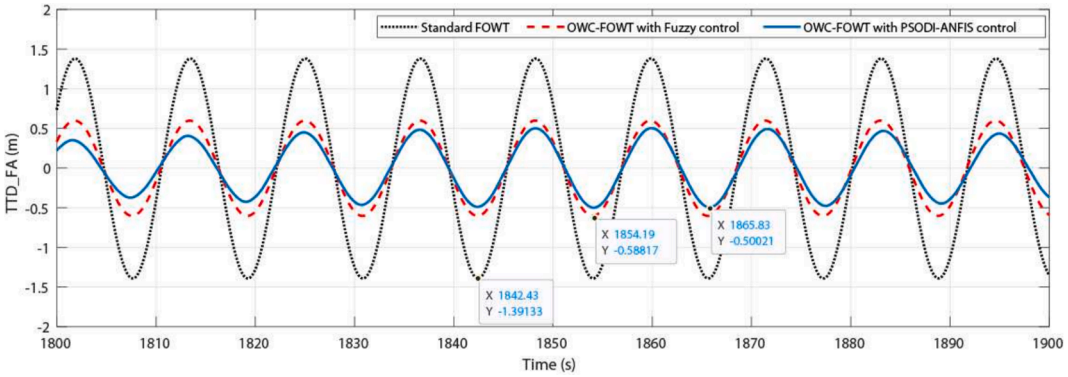

Fig. 19. TTD_{FA} for standard FOWT vs. Fuzzy-controlled OWC-FOWT and PSODI-ANFIS-controlled OWC-FOWT.

Table 7
Obtained FOWT platform modes with uncontrolled and controlled OWCs.

Modes	Platforms		
	Standard FOWT	Fuzzy-controlled OWC-FOWT	PSODI-ANFIS-controlled OWC-FOWT
Pitch (θ_p)	8.304°	3.470°	2.992°
Fore-aft (TTD_{FA})	1.3913 *m*	0.5881 *m*	0.5002 *m*

CRediT authorship contribution statement

Fares M'zoughi: Writing – review & editing, Writing – original draft, Visualization, Validation, Methodology, Investigation, Formal analysis, Conceptualization. **Izaskun Garrido:** Writing – review & editing, Writing – original draft, Visualization, Validation, Formal analysis, Conceptualization. **Aitor J. Garrido:** Writing – review & editing, Writing – original draft, Visualization, Validation, Formal analysis, Conceptualization. **Manuel De La Sen:** Writing – review & editing, Writing – original draft, Visualization, Validation, Formal analysis, Conceptualization.

Declaration of competing interest

The authors declare that they have no known competing financial interests or personal relationships that could have appeared to influence the work reported in this paper.

Data availability

No data was used for the research described in the article.

Acknowledgements

The authors would like to thank the funding entities for funding their research work through project IT1555-22 funded by the Basque Government, through grants PID2021-123543OBC21 and PID2021-123543OB-C22 funded by MICIU/AEI/10.13039/501100011033 and by ERDF/EU and the University of the Basque Country (UPV/EHU) through the María Zambrano grant MAZAM22/15 funded by UPV-EHU/MIU/Next Generation, EU.

References

[1] Jonkman JM. (2007). Dynamics Modeling and Loads Analysis of an Offshore Floating Wind Turbine; (No. NREL/TP-500-41958); *National Renewable Energy Lab. (NREL)*: Golden, CO, USA, 2007.
[2] Jonkman J, Matha D. (2010). Quantitative comparison of the responses of three floating platforms (No. NREL/CP-500-46726). *National Renewable Energy Lab. (NREL)*, Golden, CO, USA, 2010.
[3] Lackner MA. Controlling platform motions and reducing blade loads for floating wind turbines. Wind Eng 2009;33(6):541–53.
[4] Staino A, Basu B. Emerging trends in vibration control of wind turbines: a focus on a dual control strategy. Philos Trans R Soc A Math Phys Eng Sci 2015;373(2035): 20140069.
[5] Yang J, He YP, Zhao YS, Yang XY, Zhang GR. Coupled dynamic response analysis of multi-column floating offshore wind turbine with low center of gravity. J Ocean Eng Sci 2022. https://doi.org/10.1016/j.joes.2022.07.004.
[6] Lackner MA, Rotea MA. Passive structural control of offshore wind turbines. Wind Energy 2011;14(3):373–88.
[7] Luo N, Pacheco L, Vidal Seguí Y, Li H. Smart Structural Control Strategies for Offshore Wind Power generation with floating wind turbines. Renewable Energies & Power Quality Journal (RE&PQJ) 2012;1(10):1200–5.
[8] Hu Y, He E. Active structural control of a floating wind turbine with a stroke-limited hybrid mass damper. J Sound Vib 2017;410:447–72.
[9] Hu J, Zhou B, Vogel C, Liu P, Willden R, Sun K, et al. Optimal design and performance analysis of a hybrid system combing a floating wind platform and wave energy converters. Appl Energy 2020;269:114998.
[10] Sarmiento J, Iturrioz A, Ayllón V, Guanche R, Losada IJ. Experimental modelling of a multi-use floating platform for wave and wind energy harvesting. Ocean Eng 2019;173:761–73.

[11] Yu J, Li Z, Yu Y, Hao S, Fu Y, Cui Y, et al. Design and Performance Assessment of Multi-Use Offshore Tension Leg Platform Equipped with an Embedded Wave Energy Converter System. Energies 2020;13(15):3991.
[12] Gao Z, Moan T, Wan L, Michailides C. Comparative numerical and experimental study of two combined wind and wave energy concepts. J Ocean Eng Sci 2016;1 (1):36–51.
[13] Kluger JM, Slocum AH, Sapsis TP. (2017, June). A First-Order Dynamics and Cost Comparison of Wave Energy Converters Combined with Floating Wind Turbines. In *Proceedings of the 27th International Ocean and Polar Engineering Conference*, San Francisco, CA, USA, (pp. 577–585).
[14] Ma Z, Li W, Ren N, Ou J. The typhoon effect on the aerodynamic performance of a floating offshore wind turbine. J Ocean Eng Sci 2017;2(4):279–87.
[15] Slocum A, Kluger J, Mannai S. (2019, July). Energy Harvesting and Storage System Stabilized Offshore Wind Turbines. In *2019 Offshore Energy and Storage Summit (OSES)* (pp. 1-6). IEEE.
[16] Kamarlouei M, Gaspar JF, Calvario M, Hallak TS, Mendes MJ, Thiebaut F, et al. Experimental analysis of wave energy converters concentrically attached on a floating offshore platform. Renew Energy 2020;152:1171–85.
[17] Khatibani MJ, Ketabdari MJ. Numerical modeling of an innovative hybrid wind turbine and WEC systems performance: A case study in the Persian Gulf. J Ocean Eng Sci 2022. https://doi.org/10.1016/j.joes.2022.05.008.
[18] Tom NM, Lawson MJ, Yu YH, Wright AD. Development of a nearshore oscillating surge wave energy converter with variable geometry. Renew Energy 2016;96: 410–24.
[19] Li Q, Mi J, Li X, Chen S, Jiang B, Zuo L. A self-floating oscillating surge wave energy converter. Energy 2021;230:120668.
[20] Amini E, Nasiri M, Pargoo NS, Mozhgani Z, Golbaz D, Baniesmaeil M, et al. Design optimization of ocean renewable energy converter using a combined Bi-level metaheuristic approach. Energy Conversion and Management: X 2023;19:100371.
[21] Neshat M, Sergiienko NY, Nezhad MM, da Silva LS, Amini E, Marsooli R, et al. Enhancing the performance of hybrid wave-wind energy systems through a fast and adaptive chaotic multi-objective swarm optimisation method. Appl Energy 2024;362:122955.
[22] M'zoughi F, Aboutalebi P, Garrido I, Garrido AJ, De La Sen M. Complementary Airflow Control of Oscillating Water Columns for Floating Offshore Wind Turbine Stabilization. Mathematics 2021;9(12):1364.
[23] M'zoughi F, Garrido I, Garrido AJ, De La Sen M. Fuzzy Airflow-Based Active Structural Control of Integrated Oscillating Water Columns for the Enhancement of Floating Offshore Wind Turbine Stabilization. Int J Energy Res 2023;2023:1–23. https://doi.org/10.1155/2023/4938451.
[24] Aboutalebi P, M'zoughi F, Martija I, Garrido I, Garrido AJ. Switching control strategy for oscillating water columns based on response amplitude operators for floating offshore wind turbines stabilization. Appl Sci 2021;11(11):5249.
[25] Ahmad I, M'zoughi F, Aboutalebi P, Garrido I, Garrido AJ. A regressive machine-learning approach to the non-linear complex FAST model for hybrid floating offshore wind turbines with integrated oscillating water columns. Sci Rep 2023;13 (1):1499.
[26] M'zoughi F, Bouallègue S, Ayadi M, Garrido AJ, Garrido I. (2017, April). Modelling and airflow control of an oscillating water column for wave power generation. In *2017 4th International Conference on Control, Decision and Information Technologies (CoDIT)* (pp. 0938-0943). IEEE.
[27] M'zoughi F, Garrido I, Garrido AJ, De La Sen M. ANN-based airflow control for an oscillating water column using surface elevation measurements. Sensors 2020;20 (5):1352.
[28] M'zoughi F, Garrido I, Garrido AJ, De La Sen M. Self-adaptive global-best harmony search algorithm-based airflow control of a wells-turbine-based oscillating-water column. Appl Sci 2020;10(13):4628.
[29] Jonkman, J. (2008, January). Influence of control on the pitch damping of a floating wind turbine. In *Proc. IEEE 46th IEEE Aerosp. Sci. Meet. Exhibit*, (pp. 1-15). Reno, NV, USA.
[30] Stewart G, Lackner M. Offshore wind turbine load reduction employing optimal passive tuned mass damping systems. IEEE Trans Control Syst Technol 2013;21(4): 1090–104.
[31] Garrido AJ, Garrido I, Barambones O, Alkorta P, Maseda FJ. Simple linear models for plasma control in Tokamak Reactors. In: In *2008 International Conference on Control, Automation and Systems*. IEEE; 2008. p. 2429–32.
[32] Lackner MA, Rotea MA. Structural control of floating wind turbines. Mechatronics 2011;21(4):704–19.
[33] Pérez-Collazo C, Greaves D, Iglesias G. A review of combined wave and offshore wind energy. Renew Sustain Energy Rev 2015;42:141–53.
[34] Aubault A, Alves M, Sarmento AN, Roddier D, Peiffer A. (2011, January). Modeling of an oscillating water column on the floating foundation WindFloat. In *International Conference on Offshore Mechanics and Arctic Engineering* (Vol. 44373, pp. 235-246).
[35] Hu Y, Wang J, Chen MZ, Li Z, Sun Y. Load mitigation for a barge-type floating offshore wind turbine via inerter-based passive structural control. Eng Struct 2018; 177:198–209.
[36] M'zoughi F, Lekube J, Garrido AJ, De La Sen M, Garrido I. Machine learning-based diagnosis in wave power plants for cost reduction using real measured experimental data: Mutriku Wave Power Plant. Ocean Eng 2024;293:116619.
[37] Jang R. Neuro-Fuzzy Modeling: Architectures, Analyses, and Applications. Berkeley: University of California; 1992. PhD Thesis.
[38] Karaboga D, Kaya E. Adaptive network based fuzzy inference system (ANFIS) training approaches: a comprehensive survey. Artif Intell Rev 2019;52:2263–93.
[39] Kaloop MR, Bardhan A, Kardani N, Samui P, Hu JW, Ramzy A. Novel application of adaptive swarm intelligence techniques coupled with adaptive network-based fuzzy inference system in predicting photovoltaic power. Renew Sustain Energy Rev 2021;148:111315.
[40] Jang JS. ANFIS: adaptive-network-based fuzzy inference system. IEEE Trans Syst Man Cybern 1993;23(3):665–85.
[41] Mola M, Amiri-Ahouee R. ANFIS model based on fuzzy C-mean, grid partitioning and subtractive clustering to detection of stator winding inter-turn fault for PM synchronous motor. International Transactions on Electrical Energy Systems 2021; 31(3):e12770.
[42] Havens TC, Bezdek JC, Leckie C, Hall LO, Palaniswami M. Fuzzy c-means algorithms for very large data. IEEE Trans Fuzzy Syst 2012;20(6):1130–46.
[43] Setyawan AA, Ilham A. A novel framework of the fuzzy c-means distances problem based weighted distance. Applied Computing and Informatics 2019. arXiv preprint arXiv:1907.13513. 10.48550/arXiv. 1907.13513.
[44] Cebeci Z, Yildiz F. Comparison of k-means and fuzzy c-means algorithms on different cluster structures. Journal of Agricultural Informatics 2015;6(3):13–23.
[45] R.C. Eberhart and J. Kennedy, "A new optimizer using particle swarm theory," In *Proc. of the 6th Int. Symp. on micro machine and human science*, vol. 1, pp. 39-43, 1995.
[46] R.C. Eberhart and Y. Shi, "Particle Swarm Optimization: Developments, Applications and Resources," In *Proc. of the IEEE Congress on Evolutionary Computation*, pp. 81-86, Seoul, Korea, 2001.
[47] M'zoughi F, Bouallegue S, Garrido AJ, Garrido I, Ayadi M. Stalling-free control strategies for oscillating-water-column-based wave power generation plants. IEEE Trans Energy Convers 2017;33(1):209–22.